Jacob Linder and Sol H. Jacobsen

14 Spin-orbit interactions, spin currents, and magnetization dynamics in superconductor/ferromagnet hybrids

Abstract: Superconductors can enhance central effects in spintronics such as magnetoresistance and spin injection and even create conceptually new types of phenomena that have no counterpart in nonsuperconducting systems. Much like the key role that has been played by magnetic inhomogeneities in superconducting systems, recent developments suggest that spin-orbit coupling can play a similarly important part in superconducting spintronics. Here, we discuss how spin-polarized Cooper pairs can emerge from conventional *s*-wave BCS superconductors by utilizing hybrid structures with spin-orbit coupling and also highlight some recent developments in the field of nonequilibrium spin transport in superconductors. We will primarily discuss recent findings in our research group which demonstrate how spin-orbit coupling leads to novel phenomena such as spin-valve functionality with a single homogeneous ferromagnet and symmetry-protected proximity effects. We will also briefly cover results on magnetization dynamics, spin supercurrents, the consequences of domain wall motion in Josephson junctions, and how spin-transfer torques are affected by the presence of superconducting correlations.

Keywords: Superconductor, spintronics, spin-orbit coupling, magnetization dynamics, domain walls, heterostructures, proximity effects

14.1 Spin-orbit coupling from inversion symmetry breaking: novel phenomena in SF structures

Creating and manipulating spin flow is the central feature of superconducting spintronics [1]. In the presence of magnetically inhomogeneous structures, including multilayers or ferromagnets with intrinsic textures such as domain walls, spin-polarized Cooper pairs emerge [2–6] which carry both charge and spin supercurrents [7–11]. It has been shown experimentally [12–14] that a dissipationless charge current can flow through strong ferromagnets over distances that far exceed the penetration depth of conventional superconducting order into magnetic materials. This occurs precisely due to the creation of triplet Cooper pairs which are spin-polarized and insensitive to the pair-breaking Zeeman field. Triplet Cooper pairs were very recently experimentally observed spectroscopically inside a conventional superconductor [15, 16] and in

Jacob Linder, Sol H. Jacobsen, Department of Physics, NTNU Norwegian University of Science and Technology, N-7491 Trondheim, Norway. *E-mail:* jacob.linder@ntnu.no & sol.jacobsen@ntnu.no

DOI 10.1515/9783110456806-015,

the form of a paramagnetic Meissner effect [17]. It has been realized that intrinsic spin-orbit coupling arising from broken inversion symmetry offers an alternative avenue for obtaining the long-range (LR) triplet component [18, 19]. In that case the appearance of the LR component depends on the relative direction of the axis of broken inversion symmetry and the magnetization vector, with the LR triplet defined as having its spin aligned with the magnetization. This is in contrast to the short-ranged (SR) triplet component which has its spin perpendicular to the field, and is thus vulnerable to pair breaking just like conventional singlet Cooper pairs.

It would be impossible to comprehensively review all the activity in superconducting spintronics within this book chapter. Thus, *we emphasize that this chapter is not intended as a review* of past and ongoing activity in the field. Instead, we will primarily discuss some specific results on spin transport in superconductors obtained recently in our research group. The reader is assumed to have basic knowledge about the superconducting proximity effect in superconductor/ferromagnet (SF) hybrid structures. For a more detailed introduction to the underlying theory in this field, we refer to the chapter by A. Buzdin in this book and the review articles [20, 21].

14.1.1 From singlet to triplet Cooper pairs

Spin mixing and spin rotation

We start by briefly reviewing the established mechanism which allows us to pass from spinless $S = 0$, $S_z = 0$ singlet Cooper pairs to spin-polarized $S = 1$, $S_z = \pm 1$ triplet Cooper pairs, following the presentation of [1]. This occurs via a two-step procedure based on the concepts of spin mixing and spin rotation [22]. The wavefunction for a spin-singlet Cooper pair can be represented as:

$$\psi_0(\boldsymbol{k}) = \sqrt{\frac{1}{2}}(|\uparrow, \boldsymbol{k}\rangle\, |\downarrow, -\boldsymbol{k}\rangle - |\downarrow, \boldsymbol{k}\rangle\, |\uparrow, -\boldsymbol{k}\rangle) \tag{14.1}$$

where the prefactor is due to normalization. Here, we have ignored for brevity the symmetrization with respect to $\boldsymbol{k}$ which is not essential to demonstrate the spin-mixing process – it is easily reinstated by letting $\psi_0(\boldsymbol{k}) \rightarrow \psi_0(\boldsymbol{k}) + \psi_0(-\boldsymbol{k})$ so that the total wavefunction is invariant under $\boldsymbol{k} \rightarrow (-\boldsymbol{k})$. When the electrons of a Cooper pair scatter at a magnetic interface (such as in a superconductor/ferromagnet bilayer), they experience not only a shift in momentum but also a spin-dependent shift ν_σ, $\sigma = \uparrow, \downarrow$, in the phase of the wavefunction. This is a result of the Zeeman field that splits majority and minority spin carriers. Such a spin-dependent phase shift may be written as:

$$|\uparrow, \boldsymbol{k}\rangle \rightarrow e^{i\nu_\uparrow}\, |\uparrow, -\boldsymbol{k}\rangle,\ |\downarrow, \boldsymbol{k}\rangle \rightarrow e^{i\nu_\downarrow}\, |\downarrow, -\boldsymbol{k}\rangle\ . \tag{14.2}$$

Applying this to ψ_0 results in a new wavefunction which is a linear combination of a spin-singlet and $S_z = 0$ spin-triplet wavefunction $\Psi_{\mathrm{SR}} \equiv \sqrt{1/2}(|\uparrow, \boldsymbol{k}\rangle|\downarrow, -\boldsymbol{k}\rangle + |\downarrow, \boldsymbol{k}\rangle\, |\uparrow, -\boldsymbol{k}\rangle)$. The singlet and triplet parts of the wavefunction are weighted by

$\cos\Delta\nu$ and $\sin\Delta\nu$, respectively. Here, $\Delta\nu \equiv \nu_\uparrow - \nu_\downarrow$. If there are no spin-dependent phase shifts ($\Delta\nu = 0$), the triplet component is absent. The next step is to create the equal-spin triplet components $S_z = \pm 1$ which are insensitive to the pair-breaking effect of a Zeeman field as the spins of the electrons in the Cooper pair are aligned with each other. Such long-ranged triplet correlations $\Psi_{\mathrm{LR}} \equiv |\uparrow, \boldsymbol{k}\rangle\, |\uparrow, -\boldsymbol{k}\rangle$ (or $|\downarrow, \boldsymbol{k}\rangle\, |\downarrow, -\boldsymbol{k}\rangle$) can emerge by rotating or flipping one of the spins in the $S_z = 0$ triplet component. A spatially varying magnetization serves as a source for spin rotation. This can be seen by letting the quantization axis be aligned with the local magnetization direction: consider an $S_z = 0$ triplet state in a part of the system where the magnetization, and thus the quantization axis, is along the z-direction. However, in a part of the system where the magnetization points in the x-direction, the same $S_z = 0$ triplet state would look like a combination of the equal-spin pairing states $S_z = \pm 1$ from the perspective of the new quantization axis. Yet another way to view this is in terms of spin-flip scattering. Assume that there exists two magnetic regions where the magnetizations are not aligned. In that case, the second region acts as a spin-flip potential relative to the first region and enables processes such as $|\uparrow, \boldsymbol{k}\rangle \rightarrow |\downarrow, \boldsymbol{k}\rangle$ and vice versa. Such processes are in fact always present for instance in a scenario where local inhomogeneities of the magnetic moment exist near an interface. The combination of spin mixing and spin rotation processes then illustrate how the spin-singlet s-wave component of a conventional superconductor may be converted into a long-range spin-triplet component that is able to penetrate a long distance even into extreme environments such as half-metallic ferromagnets which are fully spin polarized.

Spin-orbit coupling: precession and relaxation

The above picture represents the traditionally established view that magnetic inhomogeneities are a necessary prerequisite in order to generate long-ranged spin-triplet superconducting correlations in ferromagnetic structures. However, recent developments [18, 23] have shown that there exists an alternative. If a superconducting material lacks an inversion center (either due to its crystal structure or due to the geometry of the setup) antisymmetric spin-orbit coupling such as Rashba type [24] will be present. This leads to a mixing of excitations from the two spin bands in such a manner that spin is no longer a conserved quantity. Instead, the long-lived excitations of the system now belong to pseudospin bands that are momentum-dependent combinations of the original spin species. As a consequence, the superconducting pairing state in noncentrosymmetric superconductors will intrinsically be a mixture of singlet and triplet pairing [25]. When pairing occurs between the quasiparticle excitations of a simple Hamiltonian H featuring antisymmetric spin-orbit coupling such as $H = \varepsilon_{\boldsymbol{k}} + \boldsymbol{g}_{\boldsymbol{k}} \cdot \underline{\sigma}$, where $\varepsilon_{\boldsymbol{k}}$ is the normal-state dispersion, $\underline{\sigma}$ is the Pauli matrix vector, and $\boldsymbol{g}_{\boldsymbol{k}} = -\boldsymbol{g}_{-\boldsymbol{k}}$ is a vector characterizing the spin-orbit coupling, the triplet part of the superconductivity can be described by the relation $\boldsymbol{d}(\boldsymbol{k}) \parallel \boldsymbol{g}(\boldsymbol{k})$. The notation $\underline{\ldots}$ is

used for 2×2 matrices. We have defined:

$$\boldsymbol{d}(\boldsymbol{k}) \equiv [(\Delta_{\downarrow\downarrow}(\boldsymbol{k}) - \Delta_{\uparrow\uparrow}(\boldsymbol{k}))/2, -\mathrm{i}(\Delta_{\uparrow\uparrow}(\boldsymbol{k}) + \Delta_{\downarrow\downarrow}(\boldsymbol{k}))/2, \Delta_{\uparrow\downarrow}(\boldsymbol{k})] \,. \tag{14.3}$$

This is the triplet d-vector [26] which is intimately linked to the spin of the Cooper pair state $\langle\sigma\rangle \propto \mathrm{i}\boldsymbol{d}(\boldsymbol{k}) \times \boldsymbol{d}(\boldsymbol{k})^*$. Besides its use for noncentrosymmetric superconductors, the d-vector formalism is also suitable to describe the proximity-induced triplet correlations in superconductor-ferromagnet structures. In this case, the anomalous Green's functions $f_{\sigma\sigma'}$ play the role of the gaps $\Delta_{\sigma\sigma'}(\boldsymbol{k})$ above. One may define a "proximity" triplet vector $\boldsymbol{f}$. The proximity effect between a noncentrosymmetric superconductor and a homogeneous ferromagnet will thus produce both SR and LR triplet superconductivity inside the ferromagnetic region [23].

The generation of LR spin triplets via spin-orbit coupling and homogeneous ferromagnetism has also been analyzed in terms of an analogy between, on the one hand, D'yakonov–Perel [27] spin relaxation and precession of spins in nonsuperconducting systems and, on the other hand, in diffusive systems with antisymmetric spin-orbit coupling in contact with conventional s-wave superconductors (see [18, 19] for details on this argument). In particular, one may compare the quasiclassical Usadel equation [28], which determines the superconducting pairing correlations quantified by the anomalous Green's function $\boldsymbol{f}$ in the presence of such spin-orbit interactions, with the spin diffusion equation for normal state systems, which determines the spin density $\boldsymbol{S}$. The comparison demonstrates that the spin-orbit interaction affects the components of $\boldsymbol{f}$ and $\boldsymbol{S}$ in the same way, meaning that the same mechanism which causes rotation of spin in diffusive normal metals can rotate the SR Cooper pairs to LR ones.

14.1.2 Spin-valve functionality with a single ferromagnet

An interesting consequence of the mechanism discussed in the previous section is that it should be possible to control the critical temperature T_c of a superconductor via the magnetization direction of one single ferromagnetic layer, which is not possible in the absence of SO coupling. In conventional SF structures, T_c is in fact independent of the magnetization orientation of the F layer (as long as the orbital effect of the stray field is neglected). By using a spin-valve setup such as FSF [29–33], it has been demonstrated that the relative magnetization configuration between ferromagnetic layers will tune T_c. In contrast, in the presence of SO coupling such a spin-valve effect can be obtained with a single homogeneous ferromagnet: by rotating the magnetization 90 degrees, T_c goes from a maximum to a minimum. The fact that only a single ferromagnet is required to achieve this is of practical significance since it potentially reduces the complexity associated with controlling the relative magnetization orientation in multilayered hybrid structures. Following [34], we now demonstrate precisely how this occurs.

The type of antisymmetric SO coupling (linear in momentum) we will consider here can be described by an SU(2) field $\underline{\boldsymbol{A}}$ (a vector with 2×2 matrices as components) whose mathematical form is determined by the material properties and the experimental geometry. Such an SO coupling in solids can originate from a lack of inversion symmetry in the crystal structure and can be of both Rashba and Dresselhaus type, depending on the point group symmetry of the crystal [24, 35–37]. It is also known that structural inversion asymmetry due to surfaces, either in the form of interfaces with other materials or with vacuum, can give rise to antisymmetric SO coupling of the Rashba type. In thin-film hybrids, the Hamiltonian for Rashba spin splitting is expressed by the cross product of the Pauli vector $\underline{\sigma}$ with the momentum $\boldsymbol{k}$,

$$H_R = -\frac{\alpha}{m}(\underline{\sigma} \times \boldsymbol{k}) \cdot \hat{\boldsymbol{z}}\,, \tag{14.4}$$

where α is called the Rashba coefficient, and $\hat{\boldsymbol{z}}$ denotes the axis along which inversion symmetry is broken. The Dresselhaus SO coupling is known to occur when the crystal structure lacks an inversion center, such as in zinc blende structures. For a two-dimensional (2D) electron gas (quantum well) confined in the $\hat{\underline{z}}$-direction the Dresselhaus splitting becomes (to first order $\langle k_z \rangle = 0$)

$$H_{\mathrm{D}} = \frac{\beta}{m}(\underline{\sigma}_y k_y - \underline{\sigma}_x k_x)\,, \tag{14.5}$$

where β is the Dresselhaus coefficient. A potential 2D electron gas candidate would be gallium arsenide, but the form (14.5) is a useful approximation for any 3D thin film with strong confinement in one direction. Combining both interactions, we obtain the Hamiltonian for a general Rashba–Dresselhaus SO coupling $H_{\mathrm{RD}} = \frac{k_x}{m}(\alpha\underline{\sigma}_y - \beta\underline{\sigma}_x) - \frac{k_y}{m}(\alpha\underline{\sigma}_x - \beta\underline{\sigma}_y)$. We can rewrite this by expressing the SO coupling as a background SU(2) field, i.e., an object with both a vector structure in geometric space and a 2×2 matrix structure in spin space:

$$H_{RD} \equiv -\boldsymbol{k} \cdot \underline{\boldsymbol{A}}/m\,. \tag{14.6}$$

It follows that $\underline{\boldsymbol{A}} = (\beta\underline{\sigma}_x - \alpha\underline{\sigma}_y, \alpha\underline{\sigma}_x - \beta\underline{\sigma}_y, 0)$ for the above example. Moreover, it is convenient to introduce a new notation for describing Rashba–Dresselhaus couplings, which allows us to distinguish between the physical effects that derive from the magnitude of the coupling and those that derive from which type of SO coupling we have: $\alpha \equiv -a\sin\chi$, $\beta \equiv a\cos\chi$, where we will refer to a as the *SO strength*, and χ as the *SO angle*. We see that $\chi = 0$ corresponds to a pure Dresselhaus coupling, while $\chi = \pm\pi/2$ results in a pure Rashba coupling.

The effect of spin-orbit coupling on T_{c} in SF bilayers was recently determined in [34] using quasiclassical theory and here we discuss some of the main findings. We set the material parameters to $N_0\lambda = 0.2$ for the superconductor (which is a standard choice for BCS superconductors), the exchange field $h = 10\Delta_0$ for the ferromagnet, and the interface parameter $\zeta = 3$ (the ratio of the interface and bulk resistance)

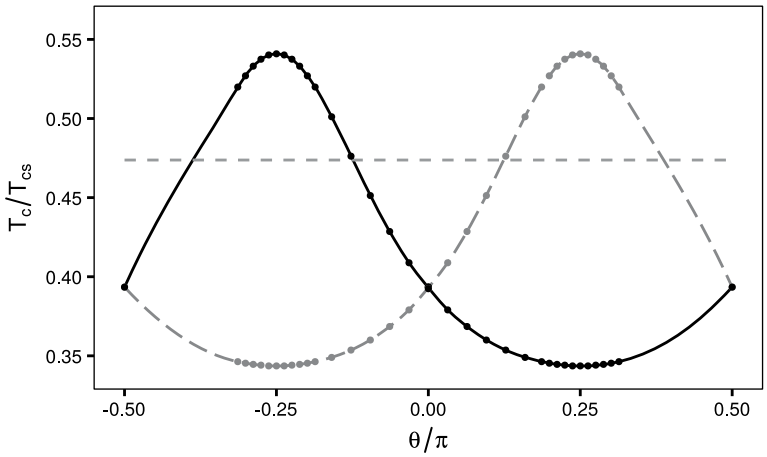

Fig. 14.1: Plot of the normalized critical temperature T_c/T_{cs} of an SF bilayer as a function of the exchange field orientation characterized by the in-plane angle θ, with $L_S/\xi_S = 0.55$, $L_F/\xi_S = 0.2$, and $a\,\xi_S = 2$. The gray dashed line corresponds to $\chi = 0$, the gray dashed line with dots is $\chi = -\pi/4$, whereas the black full line with dots is $\chi = +\pi/4$. The figure is adapted from [34].

for both materials. In Figure 14.1 the change in T_c upon varying the direction of the exchange field $\boldsymbol{h} \sim \cos\theta\hat{\boldsymbol{x}} + \sin\theta\hat{\boldsymbol{y}}$ in the xy-plane is shown. Interestingly, the critical temperature has extrema at $|\chi| = |\theta| = \pi/4$, where the extremum is a maximum if θ and χ have the same sign, and a minimum if they have opposite signs. For the choice of junction parameters chosen in Figure 14.1, this effect results in a large difference between the minimal and maximal critical temperature of nearly 60% as the magnetization direction is varied. The dependence of T_c on the magnetization orientation and the type of SO coupling can be explained from the linearized Usadel equations [34]. For certain angles θ, the SO coupling is able to rotate the $S_z = 0$ Cooper pairs into $S_z = \pm 1$ pairs and thus open an additional "leakage" channel in the proximity effect which in turn changes T_c. We will consider the properties of the linearized Usadel equations with SO coupling for a related nanowire Josephson junction in the next subsection. The variation of T_c upon changing the magnetization angle θ in the present case of an SF bilayer turns out to be strongest in the case where the Rashba and Dresselhaus magnitudes are similar. For either pure Rashba or pure Dresselhaus coupling, T_c is only affected when the magnetization acquires an out-of-plane component: pure in-plane rotations of $\boldsymbol{h}$ do not affect T_c in this scenario. The change in T_c is typically much smaller for pure Rashba coupling with an out-of-plane component of the magnetization compared with equal Rashba and Dresselhaus coupling.

14.1.3 Pure triplet proximity effect protected via parity symmetry

Phase-sensitive density of states in Josephson junctions

The superconducting proximity effect is a phase-coherent phenomenon that can be probed in e.g., Josephson junctions where the density of states (DOS) depends sensitively [38] on the superconducting phase difference ϕ. Le Sueur et al. [39] reported measurements for Josephson junctions with a normal metal (SNS) that were consistent with the prediction [40] that the DOS changes from a finite minigap due to the superconducting correlations ($\phi = 0$), with the minigap reducing as the phase difference is increased, to that of a normal metal at $\phi = \pi$. This can be understood intuitively, as the proximity effect should be suppressed when the order parameter in each superconductor is equal in magnitude but opposite in sign, resulting in superconducting correlations "averaging" to zero.

Remarkably, when SO coupling is present in a magnetic Josephson junction, the opposite effect takes place as recently shown in [41]. The SO coupling in the junction instead gives rise to a giant, triplet-induced proximity effect at $\phi = \pi$. This is shown in Figure 14.2, where the junction is oriented along the z-direction and the choice of SO coupling vector is aligned perpendicular to the interfaces ($\underline{\boldsymbol{A}}_z \neq 0$) rather than as below Equation (14.6). For concreteness and to give more transparent analytical results, we set $\underline{\boldsymbol{A}} = (0, 0, \alpha\sigma_x - \alpha\sigma_y)$. This choice corresponds e.g., to pure Rashba-type coupling with broken inversion symmetry perpendicularly to a nanowire.

The physical origin of the giant proximity effect is that SO coupling forces the triplet Cooper pairs to have the opposite parity symmetry compared to the singlet pairs with respect to the center of the junction. As will be shown below, when $\phi = \pi$ the singlet correlations are antisymmetric across the junction whereas the triplets are symmetric. This means that the proximity effect survives even in the center of the junction and is solely due to LR Cooper pairs. In other words, the experimentally tunable phase difference may be utilized to remove the spin singlets and keep only triplets even with a homogeneous exchange field. Previous attempts to separate spin-polarized Cooper pairs from the singlet component have required magnetic inhomogeneities, which can be experimentally challenging to control. Thus, the inclusion of SO coupling represents a significant step forward in this direction. Moreover, since this prediction is based solely on symmetry and that its spectroscopic fingerprint is virtually independent of where the local density of states is measured in the system, it should be very robust.

Let us first briefly consider the behavior of the proximity effect in an SFS junction without SO coupling as a function of the phase difference. In this case the quasiclassical Usadel equation [28] in the linearized regime reads

$$D_{\mathrm{F}}\partial_z^2 f_\pm + 2i\varepsilon_\pm f_\pm = 0\,, \tag{14.7}$$

where D_{F} is the diffusion constant in the ferromagnet, $\varepsilon_\pm = \epsilon \pm h_z$ and $f_\pm = f_t \pm f_s$ for energy ϵ, magnetization exchange field h, and singlet and $S_z = 0$ triplet anoma-

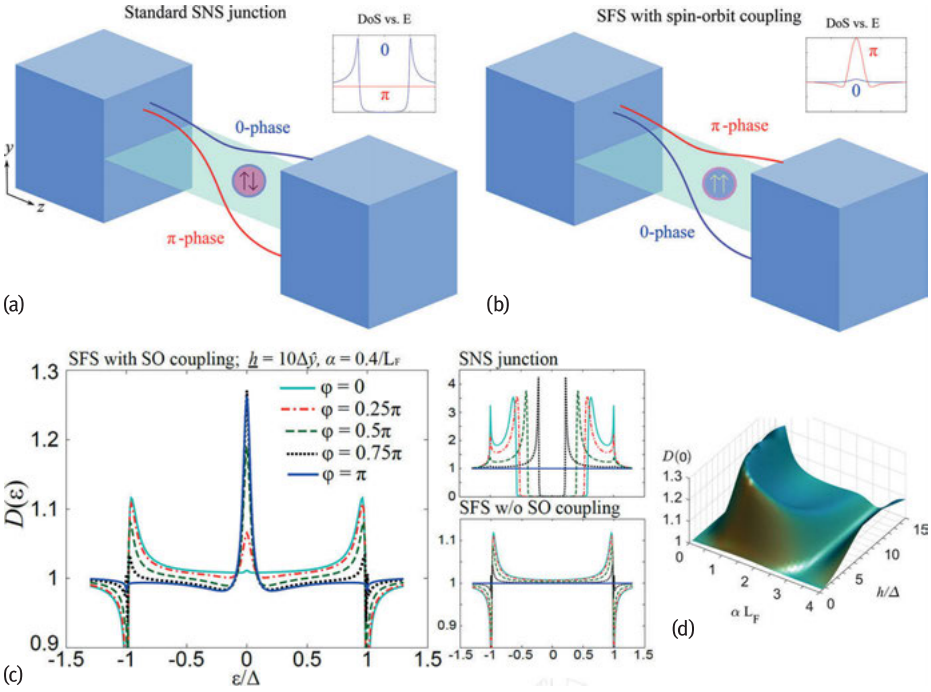

Fig. 14.2: The proximity effect in a standard SNS Josephson junction (a) results in a minigap that closes as the phase difference ϕ increases between the superconductors. The proximity effect in the SFS junction with intrinsic SO coupling (b) results in a giant zero-bias peak in the density of states when $\phi = \pi$. (c) Left figure: The local density of states $D(\epsilon)$ at $z = L_F/2$ for different values of the phase difference ϕ between the superconductors of an SFS junction with spin-orbit coupling $\underline{\boldsymbol{A}} = (0, 0, \alpha\sigma_x - \alpha\sigma_y)$, setting the exchange field $\boldsymbol{h} = 10\Delta\hat{\boldsymbol{y}}$ and the spin-orbit coupling magnitude $\alpha = 0.4/L_F$. The giant triplet proximity effect at $\phi = \pi$ manifests as a large peak in $D(\epsilon)$ at $\epsilon = 0$. Right figures: A comparison with the standard SNS and SFS junctions without SO coupling is shown. (d) The local density of states $D(\epsilon = 0)$ at $z = L_F/2$ for a π-biased SFS junction with spin-orbit coupling as a function of magnetization exchange field $\boldsymbol{h} = h\Delta\hat{\boldsymbol{y}}$ and strength of spin-orbit coupling αL_F. In all cases, the axis of broken inversion symmetry producing the spin-orbit coupling is taken to be perpendicular to the extension of the junction, i.e., for a nanowire setup. Figure is adapted from [41].

lous Green's functions f_s and f_t, respectively. The Usadel equation describes the diffusion of the condensate into the adjacent material, and the corresponding Kupriyanov–Lukichev boundary conditions [42] at the superconducting interfaces take the form $\zeta L_F \partial_z f_\pm = \mp f_{BCS} e^{i\phi_L}$ at $z = 0$ and $\zeta L_F \partial_z f_\pm = \pm f_{BCS} e^{i\phi_R}$ at $z = L_F$, where f_{BCS} is the bulk Bardeen–Cooper–Schrieffer [43] anomalous Green's function in the superconductors, L_F is the length of the ferromagnet, and ζ is the interface parameter. ϕ_L and ϕ_R denote the respective superconducting phases. The solution in the middle of the junction

reads:

$$f_{\pm} = \frac{\pm f_{\mathrm{BCS}} \cos(k_{\pm} L/2)}{\zeta L i \sin(k_{\pm} L)} (e^{i\phi_R} + e^{i\phi_L}) \,, \tag{14.8}$$

where $k_{\pm} = \sqrt{2i\varepsilon_{\pm}/D_{\mathrm{F}}}$ is the wavenumber. It follows that when the phase difference $\phi = \phi_L - \phi_R = \pi$, the superconducting proximity effect vanishes since $f_{\pm} = 0$. This holds for all energies and regardless of whether $h = 0$ or $h \neq 0$. As this takes place at $\phi = \pi$ both in SNS and SFS junctions, one might be tempted to conclude that this is a robust phenomenon. However, we now proceed to show that in the presence of spin-orbit interactions, this is no longer the case.

Symmetry-protected triplet proximity effect

To demonstrate the symmetry-protected triplet proximity effect, we follow [41] closely. This effect can be established solely on symmetry arguments, making it independent of the specific junction parameters employed in an experiment. To see this, we will analyze below the Usadel equation in the weak proximity effect limit when SO coupling is present – its Ricatti-parametrized form valid for an arbitrarily large proximity effect was derived in [34]. The nonvanishing triplet proximity effect in π-biased Josephson junctions survives even if one includes modest components of the SO coupling field $\{\underline{\boldsymbol{A}}_x, \underline{\boldsymbol{A}}_y\} \neq 0$. The origin and main features of the giant triplet proximity effect can be identified analytically by considering the low-energy regime $\varepsilon = 0$ and setting the exchange field to $\boldsymbol{h} = h\hat{\boldsymbol{z}}$. The linearized coupled Usadel equations then read:

$$\begin{aligned} (\partial_z^2 - 4\alpha^2) f_{\sigma\sigma} + 4\sigma\alpha(1 - \sigma i)\partial_z f_t - 4i\sigma\alpha^2 f_{-\sigma,-\sigma} = 0 \,, \\ D_{\mathrm{F}} \partial_z^2 f_s + 2i h_z f_t = 0 \,, \\ D_{\mathrm{F}} \partial_z^2 f_t + 2i h_z f_s - 8 D_{\mathrm{F}} \alpha^2 f_t \\ + 2 D_{\mathrm{F}} \alpha (1 - i) \partial_z f_{\downarrow\downarrow} - 2 D_{\mathrm{F}} \alpha (1 + i) \partial_z f_{\uparrow\uparrow} = 0 \,. \end{aligned} \tag{14.9}$$

with $\sigma = \uparrow, \downarrow$. At zero phase difference between the superconductors, the anomalous Green's function f_s for the singlet Cooper pairs is a symmetric function with respect to the middle of the junction. This can be seen from the general form of the solution of f_s and the boundary conditions, and is equivalent to what happens for conventional SNS and SFS junctions. When the phase difference is equal to π, however, f_s (and thus necessarily its second derivative) is antisymmetric. When the SO coupling has a component in the junction direction it necessarily introduces a first-order derivative term. If we perform the operation $z \to (-z)$ on Equation (14.9), this means that the function subject to the first-order differential must have the opposite symmetry of the other terms, provided that it is not constant. We can now see explicitly what this entails: the functions $f_{\uparrow\uparrow}$ and $f_{\downarrow\downarrow}$ must be symmetric around the middle of the junction at $\phi = \pi$, and it is clear that a nonzero component of the anomalous Green's function will remain at zero energy even in the π-biased junction while the singlet component is exactly equal to zero. The density of states at the Fermi level becomes in the linearized

regime:

$$D(0) = 1 - |f_s(0)|^2/2 + |f_t(0)|^2/2 + |f_{\uparrow\uparrow}(0)|^2/4 + |f_{\downarrow\downarrow}(0)|^2/4\,, \tag{14.10}$$

and thus an experimental signature of this effect would be an enhanced zero-energy density of states due to the triplets.

In Figure 14.2c we provide the spectroscopic profile upon varying the phase difference between the superconductors in an SFS junction with SO coupling, which highlights the emergence of a zero-energy peak in the density of states at $\phi = \pi$. We have here chosen an in-plane exchange field $\boldsymbol{h} = 10\Delta\hat{\boldsymbol{y}}$ for ease of experimental application, a bulk superconducting coherence length $\xi_S = 30$ nm and SO coupling strength $\alpha = 0.4/L_F$, i.e., normalized to the ferromagnet length L_F, here chosen to be 15 nm such that the relevant quantity $L_F/\xi_S = 0.5$. Similar behavior is observed for most of the other choices of exchange field orientation and SO coupling strength. A comparison with the standard SNS and SFS junctions without SO coupling is provided and the giant proximity effect at $\phi = \pi$ is clearly seen to be related to the presence of SO coupling. Since the singlet component f_s vanishes when $\phi = \pi$, the remaining features are entirely due to the triplets and in this case due to the LR triplet component. As a consequence, the result serves as a way to fully isolate the triplet correlations regardless of the junction parameters in π-biased Josephson junctions. We note that quantitatively, even when $h \gg \Delta$, the proximity effect and resulting enhancement of the density of states displayed here is very large ($\sim 26\%$) when compared with experiments measuring the same quantity for superconductor-ferromagnet hybrids without SO coupling [44, 45], where the deviation from the normal state is around 1%.

Although the analytical proof given above shows how 100% triplet Cooper pairs are present in the middle of the junction, numerical simulations of the full proximity effect equations show that this effect in fact turns out to be virtually independent of the distance from the superconducting interfaces: the spectroscopic peak originating from the presence of spin-polarized Cooper pairs persists all the way up to the interfaces and hardly changes throughout the junction [41]. Moreover, the spatial dependence remains unaltered even for asymmetric junctions where one interface is up to twice as transparent as the other (a ratio of barrier parameters $\zeta_1/\zeta_2 = 2$). This indicates that the predicted effect should be very robust. In Figure 14.2 we plot the dependence of the density of states of the π-biased junction on the magnitude h of the exchange field $\boldsymbol{h} = h\Delta\hat{\boldsymbol{y}}$ and the SO coupling αL_F, which is highly nonmonotonic in α. As the field strength increases, a more narrow spectrum of SO coupling will generate a giant peak at zero energy, with the optimal SO coupling decreasing slightly for higher field strengths. Nevertheless, regardless of the values of h and α, a pure triplet state is induced in the low-energy regime at $\phi = \pi$.

14.2 Controlling spin flow with superconductors

It is interesting to note that spin transport in superconductors [46–48] actually predated spin transport experiments in nonsuperconducting materials [49]. This research field has recently emerged as a potential avenue for enhancing and discovering new phenomena in spintronics. Preliminary results are indeed encouraging, with experiments demonstrating infinite magnetoresistance in superconducting spin-valves [50], strongly enhanced quasiparticle spin lifetimes [51], spin relaxation lengths [52], spin Hall effects [53], and thermoelectric currents [54] compared to nonsuperconducting structures.

14.2.1 Spin supercurrents

With regard to utilizing superconductors for spintronics purposes, the possibility of creating spin supercurrents (flowing without dissipation) in ferromagnetic materials [12] has earned the triplet Cooper pairs much attention. It is known that in the presence of inhomogeneous magnetic order, e.g., intrinsically textured ferromagnets like Ho [14, 55], or multilayers with several ferromagnets [13], triplet supercurrents can arise. This happens even when using conventional *s*-wave superconductors which feature spinless Cooper pairs (we refer the reader to the chapter by M. Blamire in this book for a much more detailed discussion on spin supercurrents from an experimental perspective). However, it can be difficult to experimentally control the magnetization direction of each of the individual layers when using large multilayered structures as in [13] to create the dissipationless spin flow. Several works have studied how triplet supercurrents can emerge in various types of structures including both weakly and strongly polarized ferromagnets (see e.g., [7–9, 56–59]). At the same time, it would be of interest if one could generate a spin supercurrent flowing in a normal (nonmagnetic) metal by using a minimal amount of magnetic elements. The reason is that this would potentially simplify the manner in which external control may be exerted on the spin supercurrent and its properties. Below, we show an example of how this can occur based on the findings of [60] where it was shown that a spin supercurrent can flow through a normal metal carried by odd-frequency triplet Cooper pairs.

A schematic of the model heterostructure used for demonstrating the spin supercurrent flow is shown in Figure 14.3. The mathematical framework takes the quasiclassical theory of superconductivity [21, 61] in the diffusive limit, where the central object of interest is the Green's matrix function $\check{g}$ which is an 8×8 matrix in Keldysh–Nambu space. It is defined in terms of the retarded (R), advanced (A), and Keldysh (K) part of the Green's function: $\check{g} = \begin{pmatrix} g^{\mathrm{R}} & g^{\mathrm{K}} \\ 0 & g^{\mathrm{A}} \end{pmatrix}$. In equilibrium, it is sufficient to consider the

retarded part $g^{\mathrm{R}} \equiv g$, which may be parametrized and normalized as [62]:

$$g = \begin{pmatrix} \underline{\mathcal{N}}(\underline{1} + \underline{\gamma}\underline{\tilde{\gamma}}) & 2\underline{\mathcal{N}}\underline{\gamma} \\ -2\underline{\tilde{\mathcal{N}}}\underline{\tilde{\gamma}} & -\underline{\tilde{\mathcal{N}}}(\underline{1} + \underline{\tilde{\gamma}}\underline{\gamma}) \end{pmatrix}, g^2 = 1 \,. \tag{14.11}$$

Here, $\underline{\mathcal{N}} = (\underline{1} - \underline{\gamma}\underline{\tilde{\gamma}})^{-1}$ and the $\tilde{\cdot}$ operation means complex conjugation and reversal of quasiparticle energy. The Ricatti matrices $\{\underline{\gamma}, \underline{\tilde{\gamma}}\}$ are 2×2 matrices in spin space and the Green's function g satisfies the Usadel equation [28]:

$$D\partial_x(g\partial_x g) + \mathrm{i}[\varepsilon\rho_3, g] = 0 \,. \tag{14.12}$$

Above, D is the diffusion coefficient of the normal metal, $\rho_3 = \mathrm{diag}(\underline{1}, -\underline{1})$, and ε is the quasiparticle energy measured relative the Fermi level. In order to account for the magnetic insulators at the interfaces shown in Figure 14.3, one uses the spin-dependent boundary conditions discussed in [63] and recently generalized to arbitrarily strong polarization in [64]. The most important effect of the magnetic insulators is the spin-dependent phase shifts experienced by quasiparticles as they scatter at the interface,

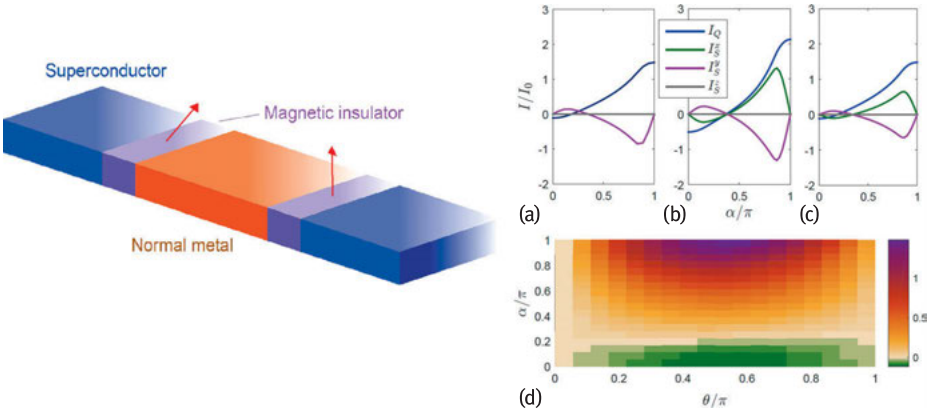

Fig. 14.3: A Josephson junction with magnetic insulators (MIs) inserted between the superconductors and the normal metal. The magnetic moments of the MIs on the left and right side of the junction, $\mathbf{m}_L$ and $\mathbf{m}_R$, may be misaligned and an applied superconducting phase difference across the junction drives both a charge and spin supercurrent. (a–d) Plot of the spin and charge supercurrents in the system where $\xi_S = 30$ nm and a normalized temperature $T/T_c = 0.02$. The interface parameters are set to be equal, $G_\varphi = 3$ and $\zeta = 2$, and the phase difference $\theta = \pi/2$. In (a), we have set $d = 20$ nm, $\phi = 0$. In (b), we have $d = 5$ nm and $\phi = \pi/4$, and in (c), we have $d = 20$ nm and $\phi = \pi/4$. The components of the spin supercurrents are mirror images of each other in (b) and (c) because of the choice of magnetic configuration of the insulators, $\phi = \pi/4$. The charge supercurrent is independent of ϕ, but changes sign when going from $\alpha = 0$ to $\alpha = \pi$, signalling a 0-π transition. The normalization constant of the charge current is $I_0 = N_0 eDA/4$ while for the spin currents it is $I_0 = N_0\hbar DA/8$. The contour plot in the bottom panel (d) is the charge supercurrent in the θ-α plane using $d = 20$ nm, displaying a 0-π transition around $\alpha \simeq 0.2\pi$ (the dark green region corresponds to the π-phase). Figure is adapted from [60].

which are described by a parameter G_φ. The superconducting regions on the left and right side of the junction are denoted g_L and g_R, and assumed to act as bulk reservoirs such that

$$\underline{\gamma}_j = \mathrm{i}\underline{\sigma}_y s/(\underline{1} + \underline{1}c)\mathrm{e}^{\mathrm{i}\theta_j},\ \underline{\tilde{\gamma}}_j = -\mathrm{i}\underline{\sigma}_y s/(\underline{1} + \underline{1}c)\mathrm{e}^{-\mathrm{i}\theta_j}\ , \tag{14.13}$$

with $j = \{L, R\}$. We have introduced $s = \sinh\Theta,\ c = \cosh\Theta$, with $\Theta = \mathrm{atanh}(\Delta_0/\varepsilon)$, where Δ_0 is the magnitude of the superconducting order parameter. The superconducting phase difference across the junction is defined as $\theta \equiv \theta_R - \theta_L$ (note that we here use θ for the phase difference instead of ϕ as before, since ϕ in the present system characterizes the magnetization orientation of the interfaces, i.e., in the xy-plane). Moreover, the angle α in this case denotes the misalignment between the two magnetic moments. For a metal of length d, the boundary conditions read $2d\zeta_L g\partial_x g = [g_\mathrm{L}, g] + \mathrm{i}G_\varphi^L[\mathcal{M}_L, g]$ at $x = 0$ and a similar one applies at $x = d$, where $\zeta_j = R_{B,j}/R_\mathrm{N}$ is the ratio between the normal-state barrier resistance on side j and the resistance of the normal metal. The matrix $\mathcal{M}_j$ describes the orientation of the magnetization of the magnetic insulator on side j. Experimentally, one would expect that the magnetic insulators will have exchange fields lying in the plane perpendicular to the tunneling direction due to shape anisotropy. The right interface magnetization is set to $\mathcal{M}_R = \mathrm{diag}(\underline{\sigma}_z, \underline{\sigma}_z)$ whereas the left interface is allowed to have an arbitrary orientation, i.e., $\mathcal{M}_L = \cos\alpha\mathrm{diag}(\underline{\sigma}_z, \underline{\sigma}_z) + \sin\phi\sin\alpha\mathrm{diag}(\underline{\sigma}_y, -\underline{\sigma}_y) + \cos\phi\sin\alpha\mathrm{diag}(\underline{\sigma}_x, \underline{\sigma}_x)$. A detailed analysis of how nonideal effects such as spin-flip scattering due to magnetic impurities and spin-orbit impurity scattering influence the charge and spin supercurrent was reported in [60].

We proceed to discuss how the charge and spin supercurrents in the system are influenced by the presence of the ferromagnetic insulators. In the quasiclassical framework, one finds:

$$I_\mathrm{Q} = \frac{N_0 eDA}{4}\int_{-\infty}^{\infty}\mathrm{d}\varepsilon\mathrm{Tr}\{\rho_3(\check{g}\partial_x\check{g})^\mathrm{K}\},\ I_\mathrm{S}^\nu = \frac{N_0\hbar DA}{8}\int_{-\infty}^{\infty}\mathrm{d}\varepsilon\mathrm{Tr}\{\rho_3\tau_\nu(\check{g}\partial_x\check{g})^\mathrm{K}\}\ . \tag{14.14}$$

We have introduced N_0 as the density of states at the Fermi level in the normal state, e is the electric charge, $\hbar$ is the reduced Planck constant, and A is the interfacial contact area. We also define the bulk superconducting coherence length $\xi_\mathrm{S} = \sqrt{D/\Delta_0}$. In the weak proximity effect regime, it is possible to compute an analytical expression for the supercurrents [60]. The charge supercurrent reads:

$$I_\mathrm{Q} = (I_{\mathrm{Q},0} + I_{Q,1}\cos\alpha G_\varphi^L G_\varphi^R)\sin\theta\ , \tag{14.15}$$

where $I_{\mathrm{Q},0}$ and $I_{Q,1}$ are lengthy expressions that depend on junction parameters such as the width d, misalignment angle α, temperature T, and the interface transparencies $\zeta_{L/R}$. The charge supercurrent is thus independent of which orientation the magnetic moments have in the xy-plane, ϕ. We see that the presence of magnetic insulators coupled to the superconductors introduces a $\cos\alpha$-dependence on the supercurrent,

which tunes its overall magnitude and also can change the quantum ground state of the junction from 0 to π when $I_{Q,1}\cos\alpha G_\varphi^L G_\varphi^R = -I_{\mathrm{Q},0}$. Thus, 0-$\pi$ transitions may occur by changing α. As seen in Figure 14.3d, the charge supercurrent changes sign at $\alpha \simeq 0.2\pi$ corresponding to the 0-π crossover, demonstrating that this is a robust feature in the full proximity effect regime.

It turns out that there exists not only a superflow of charge in the system, but also of spin. The spin supercurrent is polarized in the direction $\mathbf{m}_L \times \mathbf{m}_R$. For our setup, it means that while $I_{\mathrm{S}}^z = 0$, one has:

$$I_{\mathrm{S}}^x = G_\varphi^L G_\varphi^R \sin\phi \sin\alpha (I_{S,0} + I_{S,1}\cos\theta)\,. \tag{14.16}$$

It follows that the spin supercurrent vanishes if one only has one magnetic insulator, in which case G_φ^L or G_φ^R is zero. Moreover, it is proportional to $\sin\alpha$, which shows that it is also absent in the parallel (P) or antiparallel (AP) alignment ($\alpha = 0, \pi$). For other angles α, however, it is present. The coefficients $\{I_{S,0}, I_{S,1}\}$ are purely real and vanish when $\Delta = 0$, demonstrating that this spin supercurrent originates from the presence of superconductivity. There exists a simple relation between the components of the spin supercurrent in the xy-plane, $\frac{I_{\mathrm{S}}^x}{I_{\mathrm{S}}^y} = -\frac{\sin\phi}{\cos\phi}$. This spin supercurrent has several interesting features. Firstly, it is conserved throughout the normal metal just like the charge current. Secondly, it is long-ranged as it flows through a normal metal without any exchange field which has a pair-breaking effect on Cooper pairs. Thirdly, it has one component that is independent of the superconducting phase difference θ. The other component goes like $\cos\theta$, meaning that the total spin supercurrent satisfies $I_{\mathrm{S}}^x(\theta) = I_{\mathrm{S}}^x(-\theta)$. Note that a pure spin current is invariant under time-reversal symmetry, $\theta \to (-\theta)$, unlike a charge supercurrent which changes sign under the same operation.

14.2.2 Enhanced spin lifetimes and relaxation lengths in superconductors

Whereas the first studies of spin imbalance in superconducting spin-valves assumed that the spin lifetime in the superconducting state τ_s was unaltered compared with the normal state τ_n, experiments have since then demonstrated strongly enhanced quasiparticle spin lifetimes in the superconductors. Yang et al. [51] reported spin lifetimes in superconducting Al that exceeded their normal state values by a factor of 10^6. They inferred this by measuring a tunnel magnetoresistance due to spin imbalance that was consistent with precisely such a large spin lifetime. The spin-charge separation, which we will discuss in more detail below, and reduced spin-orbit scattering rate near the gap edge for quasiparticles in a superconductor leads to increased spin lifetimes compared to the normal state due to their movement slowing down for $E \simeq \Delta$ (we use E for the quasiparticle energy here to more easily distinguish it from the normal-state band dispersion $\varepsilon_{\boldsymbol{k}}$). A key aspect of the work by Yang et al. was that the enhancement of the spin lifetime in the superconductor relative to the normal state increases greatly when taking into account impurity spin-orbit scattering [51]. When doing so, the rela-

tive spin susceptibility χ_S/χ_N remains finite as $T \to 0$. A treatment without spin-orbit effects, in contrast, provides a considerably smaller increase of the spin lifetime in the superconducting state [65].

Quasiparticles in a superconductor can be described by 4×1 spinors in particle-hole and spin space. These excitations are in general mixtures of electron- and hole-states, but are typically characterized as being electron- or hole-like depending on the limiting value of the wavefunction for energies $E \gg \Delta$. An electron-like quasiparticle with spin-$\uparrow$ can be expressed as $\psi = [u, 0, 0, v]^T e^{iq_e x}$, where $u = \sqrt{\frac{1}{2}[1 + \sqrt{E^2 - \Delta^2}/E]}$ and $v = \sqrt{\frac{1}{2}[1 - \sqrt{E^2 - \Delta^2}/E]}$. For $E \gg \Delta$, $u \to 1$, and $v \to 0$. The wavenumber of an electron-like excitation reads $q_e = \sqrt{2m(\mu + \sqrt{E^2 - \Delta^2})}$ for a simple parabolical normal-state dispersion relation $\varepsilon_q = q^2/2m^*$ where m^* is the effective mass. In order to obtain information about the spin and charge content of these excitations, let us introduce the operators:

$$\hat{\mathbf{S}} = \frac{\hbar}{2}\begin{pmatrix} \sigma & \mathbf{0} \\ \mathbf{0} & -\sigma^* \end{pmatrix}, \ \hat{Q} = -|e|\begin{pmatrix} \mathbf{1} & \mathbf{0} \\ \mathbf{0} & -\mathbf{1} \end{pmatrix}, \tag{14.17}$$

where $|e|$ is the magnitude of the electron charge and σ is a vector with the Pauli spin matrices. Calculating the expectation values for spin and charge using the wavefunction ψ above produces:

$$\langle \hat{\boldsymbol{S}} \rangle = (\hbar/2)\hat{\boldsymbol{z}}, \ \langle \hat{Q} \rangle = -|e|\sqrt{E^2 - \Delta^2}/E \, . \tag{14.18}$$

We see that while the spin of quasiparticles is independent of their energy, the effective charge significantly depends on the excitation energy E: in particular, it vanishes near the gap edge $E \to \Delta$. This is the crucial property of the excitations which leads to spin-charge separation and longer spin lifetimes in superconductors. The group velocity $v_g = \frac{\partial E}{\partial k} = \frac{k}{m^*}\frac{\varepsilon_k - \mu}{E}$ of the excitation $E = \sqrt{(\varepsilon_k - \mu)^2 + \Delta^2}$ is also reduced at the gap edge since $E \to \Delta$ requires $(\varepsilon_k - \mu) \to 0$. This causes scattering to occur less frequently so that the lifetime increases.

When it comes to spin-current injection into superconducting spin-valves hosting ferromagnet leads, the spin imbalance in the superconductor depends on the magnetization configuration. We follow here the argument presented in [66]: let τ_s be the spin relaxation time inside the superconductor while τ_t and τ_E are the time between two tunneling events and the energy relaxation time for quasiparticles, respectively. If one assumes that $\tau_E < \tau_s < \tau_t$, the physical scenario is that electrons tunnel into the superconductor from a ferromagnetic lead, keeping their spin orientation whilst there but energetically relaxing into the equilibrium (Fermi) distribution function before leaving the superconductor. When the superconductor has a smaller thickness than the spin diffusion length, the spin-$\uparrow$ and spin-$\downarrow$ distribution functions for quasiparticles will be spatially uniform and described by the Fermi function $f(E)$, albeit with shifted chemical potentials. This shift depends on whether the magnetization configuration

of the spin-valve is parallel or antiparallel. In the P alignment, the spin conductances G_σ are equal at both interfaces due to the symmetry of the setup. Consequently, there is no net shift $\delta\mu$ in the chemical potential for the spin species σ and thus no spin accumulation in the superconductor. This changes if the alignment is changed to AP: the different density of states for spin-↑ and spin-↓ at the two interfaces produces imbalanced spin currents and yields a net shift in the chemical potential for spins σ inside the superconductor. This is expressed mathematically as $f_\uparrow(E) = f_0(E - \delta\mu)$ and $f_\downarrow(E) = f_0(E + \delta\mu)$. By considering the self-consistency equation for the superconducting order parameter

$$1 = gN_0 \int_0^{\omega_D} \mathrm{d}\varepsilon E^{-1}(1 - f_\uparrow - f_\downarrow)\,, \tag{14.19}$$

one observes that the spin-discriminating shift in chemical potential plays the same role as a Zeeman splitting $\mu_\mathrm{B}H$ originating from an external field H. This is known to cause a first-order phase transition at the Clogston–Chandrasekhar [67, 68] field $\mu_\mathrm{B}H = \Delta_0/\sqrt{2}$. Here, ε is the normal-state band energy, g is the pairing potential causing superconductivity, N_0 is the normal-state density of states at the Fermi level, μ_B is the Bohr magneton, while ω_D is the cut-off frequency for the bosons composing the superconducting glue.

Using a different setup from Yang et al., by employing an intrinsic Zeeman splitting in the superconducting region via in-plane magnetic fields, Quay et al. [52] demonstrated experimentally a nearly chargeless spin imbalance in superconducting Al using a spin-valve setup with Co as the ferromagnetic material. Measuring the nonlocal resistance due to diffusion of the spin imbalance signal yielded very different timescales for spin and charge relaxation: 25 ns versus 3 ps. Moreover, their results indicated a strongly enhanced spin lifetime in the superconducting state. A key reason for the strong spin accumulation when the tunneling from an F electrode matched the gap edge for one of the spin carriers was the intrinsic spin splitting of the density of states. Similar conclusions were also reported by Hübler et al. [69].

The field of nonequilibrium spin transport in superconductors has very recently seen two additional pivotal discoveries, namely the observation of a giant spin Hall effect in a superconductor [53] and large thermoelectric currents in a Pauli-limited superconductor [54]. It deserves special mention that the change in spin-relaxation length λ_sf in the superconducting state compared to the normal state as one decreases the temperature below T_c does depend on the origin of the spin-flip processes. For spin-orbit scattering via impurities, λ_sf is the same both above and below T_c [65]. In contrast, Poli et al. [70] observed a reduction of λ_sf by roughly an order of magnitude in the superconducting state. This was explained in terms of spin-flip scattering originating from magnetic impurities [71]. The value of the spin-relaxation length was obtained by nonlocal resistance measurements that detected the diffusion of the spin imbalance originating from the spin injection point. Finally, we also note that spin absorption by superconductors with strong spin-orbit coupling has been demonstrated

by Wakamura et al. [72], where the observed spin relaxation time was much larger in the superconducting state of Nb than in its normal state.

It is clear that spin transport in superconductors offers several key advantages compared to nonsuperconducting structures and we speculate that some of the most important advances in the field of superconducting spintronics in the upcoming years will be done precisely in the realm of nonequilibrium spin flow in superconducting hybrid structures.

14.3 Magnetization dynamics and spin torques in superconductors

By now, long-range triplet supercurrents propagating a distance $\gg \xi_F$ (with ξ_F being the ferromagnetic coherence length) through strong or even half-metallic ferromagnets have been demonstrated by several groups. However, the fact that these currents are spin-polarized is only inferred indirectly through these measurements via their long range. It would be very interesting to obtain more direct proof of the most interesting quality of such triplet currents – their spin. In conventional spintronics, spin currents are responsible for phenomena such as spin-transfer torque and magnetization switching. Observing these central effects induced via triplet supercurrents would directly prove their spin-polarized nature and represent a considerable advance toward possible cryogenic applications. The study of magnetization dynamics in superconducting structures is at an early stage, especially from the experimental side (although progress has recently been made [73]), which means that there remains much exciting work to be done in this particular area of superconducting spintronics.

14.3.1 Domain wall motion in superconducting structures

Magnetic domain wall motion is a major research topic in spintronics as it provides an innovative way of transmitting and storing information in a nonvolatile manner. In [74], it was shown that domain wall motion in superconducting hybrid structures can control whether or not the system resides in a dissipationless state by actually switching on or off superconductivity. Enhancing supercurrents through the creation of triplet Cooper pairs by utilizing magnetic domain walls was experimentally demonstrated in [75]. To model a domain wall, one minimizes the free energy functional for a ferromagnet by including the exchange stiffness and anisotropy:

$$\mathcal{F} = \int \mathrm{d}x[A(\partial_x \boldsymbol{M})^2/2 - K_{\mathrm{easy}} M_z^2 + K_{\mathrm{hard}} M_x^2] \,. \tag{14.20}$$

A is the exchange stiffness and K_{easy} and K_{hard} are the anisotropy energies associated with the easy and hard axes of the magnetization, $\boldsymbol{M}$. The result [76] is $\boldsymbol{M}(x) =$

$M_0[0, \sin\theta(x), \cos\theta(x)]$ where the parameter $\theta(x)$ determines the spatial profile of the domain wall: $\theta(x) = 2\arctan\{\exp[(x - X)/\lambda]\}$, with $\lambda = \sqrt{A/K_{\text{easy}}}$ being the domain wall width. The motion of the domain wall is described by the time-dependence of its center-coordinate $X = X(t)$. Inserting this magnetization profile into the equations of motion for the Green's function (for instance the Usadel [28] equation in the diffusive limit) enables us to calculate the supercurrent response of the system. In the ballistic regime, one makes use of the microscopic Bogoliubov–de Gennes (BdG) technique [98]. Determining the self-consistent ground state of the SFS system requires a calculation of the free energy, $\mathcal{F}$, whereafter the supercurrent can be found by: $j_x = 2e(\partial\mathcal{F}/\partial\phi)/\hbar$, where ϕ is again the superconducting phase difference.

In order to highlight the interesting consequences of domain wall motion in superconducting junctions, Linder and Halterman [74] begin by demonstrating the possibility of 0-π transitions triggered solely by the position of the wall. In Figure 14.4(a) and (b) the critical current in the diffusive regime of transport is shown. Two different parameter sets have been used for the sake of showing that this effect does not just occur for special, finely tuned parameters. The domain wall position in the ferromagnet is denoted by X. In all plots, the transition is clearly seen. Figure 14.4 shows that the domain wall movement is able to induce 0-π transitions for strong exchange fields. In fact, one should expect to see 0-π oscillations induced by even smaller increments of the domain wall position X as the exchange field is raised, precisely as seen when comparing Figure 14.4a and b. We underline that the calculation is done for a scenario where the system has relaxed to equilibrium with the domain wall at position X in the junction. Computing the supercurrent value versus X then corresponds to performing multiple measurements of the current (yet within one single sample) with the domain wall at rest in different positions. We later comment on how this can be accomplished experimentally. It would be of great interest to perform a real-time calculation of the domain wall propagation through the Josephson junction (although this is a rather complex problem).

What is the physical origin of the influence of the domain wall on the superconducting state? This may be most easily understood by first considering a limiting case of a thin domain wall in the ballistic limit. In this case, the ferromagnetic region can be viewed as an effective bilayer of two oppositely aligned ferromagnets. Now, whether the ground state is 0 or π is determined by the total phase shift accumulated as an Andreev bound state carrying the supercurrent propagates through the ferromagnet. This phase shift depends on both the length of the system and, importantly, the texture of the magnetization. For a system comprised of two ferromagnets with antiparallel alignment, the phase shift is partially canceled by the two layers. In fact, when the two domains have exactly the same width, one would expect the system to be practically equivalent to an SNS system resulting in a 0-phase [78]. In contrast, if the layers are allowed to have different thicknesses, the phase shift picked up by the Andreev bound state will allow for a π-state to be sustained as long as h and/or L are sufficiently large to generate a π-phase difference as the bound state makes a full round-trip between

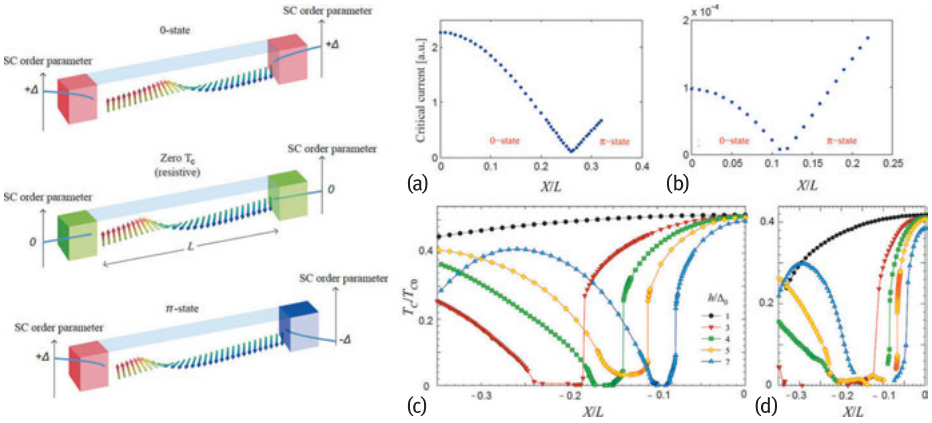

Fig. 14.4: Left panels: In a ferromagnetic layer of width L, a domain wall is present and separates two conventional s-wave superconductors. Inducing domain wall motion to a new position triggers a change in the quantum ground state of the junction: a 0-π transition. Moreover, transporting the domain wall changes the critical temperature T_c and may even reduce it to zero (middle figure), destroying completely the superconducting order. The domain wall can be manipulated via an electric current, external field, or spin-wave excitations and moved to specific locations by artificially tailored pinning sites e.g., via geometrical notches in the sample. Right panel: Critical current for two different parameter sets are shown in: (a) $h/\Delta = 8$, $\lambda/L = 0.05$, $L/\xi = 1.5$ and (b) $h/\Delta = 30$, $\lambda/L = 0.1$, $L/\xi = 1$. We have used an interface parameter $\zeta = 4$ (relatively low interface transparency and a temperature $T/T_c = 0.1$. (c) Turning superconductivity on or off: Critical temperature for an SFS junction as a function of domain wall position for several different exchange fields (see legend). It is assumed here that $\lambda/L = 0.02$, $d_S = 0.95\xi$, $L/\xi = 1$, and $Z_B = 0$. (d) Critical temperature versus domain wall position for an S/F bilayer. The same parameter values that were used in (c) have been used apart from the superconductor width which was set to $d_S = \xi$. Figure is adapted from [74].

the superconducting regions. Based on this picture, we are in a position to understand why moving the domain wall will induce 0-π transitions. The net phase shift experienced by the Andreev bound state as it propagates between the superconductors is determined by the position of the domain wall. When the domain wall has a finite width, the analogy to a bilayer breaks down since spin rotation takes place and a magnetization component perpendicular to the easy axis exists close to the domain wall center. It was verified in [74] that the domain wall position still determines whether the junction is in a 0- or π-state in the case where the domain wall extends over a large part of the junction. The position of the domain wall can also be used to control T_c, both in a Josephson junction setup and a bilayer (here shown in Figure 14.4c and d for the ballistic limit), when the superconductor thickness is of order ξ_S. Connecting with the experimental arena, we note that weak exchange fields of order a few Δ (corresponding to ~ 5 meV) have been reported in weak PdNi ferromagnetic alloys [77]. Moreover, the bulk superconducting coherence length can exceed 100 nm in dirty bulk superconductors such as Al. The parameter sets used in Figure 14.4 are thus accessible experimentally.

It has been theoretically shown that spin-triplet superconducting correlations can induce magnetization dynamics and spin-transfer torques [79–83], and one may by extension expect that domain wall motion in a Josephson junction can be induced by a supercurrent-induced spin-transfer torque as well. The required current densities to move domain walls are typically of order 10^4–10^5 A/cm^2, which compare well with the critical current density attainable in SFS junctions [84]. Once domain wall motion has been induced, artificially tailored pinning sites may be used to control where the motion terminates. In turn, this induces a new ground-state configuration. This is done experimentally by e.g., making geometrical notches at the desired locations of the ferromagnet [85]. Regarding candidate materials for observation of the predicted effects, one would need two standard s-wave superconductors, such as Nb or Al, and a magnetic region supporting a domain wall with a width of order 5–10 nm. Such magnetic textures are known to occur in thin magnetic films Pt/Co/AlO$_x$, PtI(Co/Pt)$_n$, and (Co/Ni)$_n$ (see e.g., [86]). It might also be possible to use standard ferromagnets such as Fe, Co, Ni, and their alloys that typically feature domain walls which are several tens and up to a hundred nanometers, if one is able to reduce the wall thickness by reinforcing shape anisotropy in magnetic nanowires [87]. It is clear that domain wall motion would necessitate a nonequilibrium supercurrent setup.

14.3.2 Magnetization switching and φ_0-states in Josephson junctions

Several theoretical works have demonstrated that triplet supercurrents can indeed induce spin-transfer torque switching [79, 80] and magnetization dynamics in the superconducting state [81, 83, 88–90]. Furthermore, the influence of superconductivity on spin-pumping effects have been theoretically investigated both in Josephson junctions [91] and in SF bilayers [92]. The prediction of features such as φ_0-states, which have a single but arbitrary ground state can provide direct coupling between the supercurrent and the magnetic moment in the interstitial junction material [93], and suggests many resources for spintronic manipulation.

We here provide an example of how magnetization dynamics for a Josephson junction can be computed, considering an interstitial ferromagnetic trilayer. The geometry is chosen so that the structure is positioned along the y-axis with interfaces that lie in the x–z-plane. Let $y = 0$ be the interface between the left superconducting layer and its proximate ferromagnet. Assuming large superconducting reservoirs with size $d \gg \xi_S$, these layers are characterized by their bulk superconducting gap Δ and the macroscopic phase difference across the junction, $\phi = \phi_R - \phi_L$. In order to capture the magnetization dynamics, we allow for an arbitrary direction of the magnetization in the free layer and fix the orientation in the two hard magnetic layers to the z- and x-axis, respectively. The three ferromagnetic layers $j \in \{1, 2, 3\}$ are described by their thickness L_j and the magnitudes of their exchange field h_j. The role of the interface re-

sistance is captured via an effective dimensionless parameter Z (see the seminal BTK-paper [94]).

The rich physics involving supercurrent-induced magnetization reversal and the appearance of a φ_0-ground state are both intimately linked to chiral spin symmetry breaking by the magnetization vectors $\boldsymbol{M}_j$ [95, 96]. This is quantified by a finite value of the chirality vector:

$$\chi = \boldsymbol{M}_1 \cdot (\boldsymbol{M}_2 \times \boldsymbol{M}_3) \,. \tag{14.21}$$

Once $\chi \neq 0$, spin chirality symmetry is broken. It was argued in [97] that when this happens, it induces an asymmetry between tunneling probabilities for left- and rightward motion at the interfaces even at zero phase difference. Because of this asymmetry, a finite supercurrent can flow even at $\phi = 0$. The starting point for the computation of the supercurrent-induced domain wall motion is the mean-field Bogoliubov–de Gennes equations [98] describing quasiparticle propagation in these structures. The free layer magnetization is allowed to take arbitrary directions. This enables a study of the supercurrent-induced dynamics of the magnetic order parameter of this layer. The Andreev levels ε responsible for the supercurrent in the short-junction regime $L \ll \xi$ will depend on the junction geometry, the $U(1)$ superconducting phase gradient, and the magnetization texture. When these are specified, the free energy $\mathcal{F}$ and the charge supercurrent $\mathcal{I}$ are obtained via [99]:

$$\mathcal{F}(\phi) = -\frac{1}{\beta}\sum_j \ln(1 + \mathrm{e}^{-\beta\varepsilon_j}), \;\; \mathcal{I}(\phi) = \frac{2e}{\hbar}\sum_i f(\varepsilon_i)\frac{\partial \varepsilon_i}{\partial \phi} \,, \tag{14.22}$$

where $f(\varepsilon)$ is the Fermi–Dirac distribution function and $\beta = 1/k_{\mathrm{B}}T$. There exists an interesting co-dependence between the superconducting phase difference ϕ and the noncollinearity of the magnetization vectors when it comes to determining the supercurrent $\mathcal{I}$ and the equilibrium magnetic torque τ, which was first noted in [79]. Considering for simplicity two monodomain ferromagnets with magnetizations that are aligned with a relative angle θ between each other. In this system, it follows from $\mathcal{I} = \frac{2e}{\hbar}\frac{\partial \mathcal{F}}{\partial \phi}$ and $\tau = \frac{\partial \mathcal{F}}{\partial \theta}$ that:

$$\frac{\partial \mathcal{I}}{\partial \theta} = \frac{2e}{\hbar}\frac{\partial \tau}{\partial \phi} \,. \tag{14.23}$$

Despite its compact form, the above equation contains a powerful result: if the supercurrent responds to a change in the magnetization orientation θ, then the torque exerted on the magnetic order parameters is also sensitive to a change in the phase difference ϕ. This is a basic principle enabling supercurrent-induced magnetization dynamics in inhomogeneous SFS junctions. An important point worth emphasizing is that a long-ranged triplet current does *not* induce magnetization dynamics in the layer it is propagating in. The reason is simply that such a current is spin-polarized along the magnetization direction and hence acts with no torque on the magnetic order parameter. Instead, as recently shown in [100], there is a unique interference effect between long- and short-ranged Cooper pairs that give rise to different types of superconductivity-induced magnetic torques.

Once the free energy of the system is obtained from the Andreev levels, one can derive the effective field $\boldsymbol{H}_{\text{eff}}$ which couples to the magnetization:

$$\boldsymbol{H}_{\text{eff}} = -\frac{1}{V}\frac{\partial \mathcal{F}}{\partial \boldsymbol{M}} \,. \tag{14.24}$$

The supercurrent-induced magnetization dynamics in the free layer is determined by solving the Landau–Lifshitz-Gilbert (LLG) equation [101]:

$$\frac{\partial \boldsymbol{M}}{\partial t} = -\zeta \boldsymbol{M} \times \boldsymbol{H}_{\text{eff}} + \alpha \boldsymbol{M} \times \frac{\partial \boldsymbol{M}}{\partial t} \,, \tag{14.25}$$

where ζ is the gyromagnetic ratio and α is the Gilbert damping constant. So long as the effective field is not completely aligned with the magnetization, it will exert a torque on it. Note that we are here considering a monodomain model for the soft ferromagnetic layer, meaning that there exists no contribution from the spin stiffness term $\sim \frac{\partial^2 \boldsymbol{M}y}{\partial y^2}$. However, we do include the influence of magnetic anisotropy via additional terms $\pm K_j M_j^2$, $j \in \{x, y, z\}$ in the free energy where K_j are the anisotropy densities and the $\pm$ sign determines the hard and easy axes of magnetization.

A generally valid expression for the Andreev bound-state (ABS) spectrum in the system under consideration does not have an analytically manageable form. However, physical insight can be obtained in experimentally relevant limiting cases. For instance, in the quasiclassical limit of a rather weak ferromagnet $h/\mu \ll 1$, one finds:

$$\varepsilon_{\pm} = \Delta_0 \sqrt{1 - \mathcal{A}\cos\phi + \mathcal{B}Z^3(h_y/h)\sin\phi - \mathcal{C} \pm \sqrt{\mathcal{D}(\phi)}} \,, \tag{14.26}$$

where the coefficients $\mathcal{A}, \mathcal{B}, \mathcal{C}$ are independent of the phase difference ϕ. Instead, they are functions of the system parameters such as length L, barrier Z, and exchange field h. It should be noted that Equation (14.26) is valid for arbitrary interface transparency Z. Interestingly, it follows from the above properties of the Andreev level [83] that there will be a finite supercurrent at zero phase difference: the system is in a φ_0-state. Very recently, the first experimental evidence for such a Josephson junction was put forth [97]. Note that the Andreev levels satisfy in general $\varepsilon(\phi) \neq \varepsilon(-\phi)$.

The existence of an anomalous current at zero phase difference is seen to require two criteria to be fulfilled: 1) the presence of scattering barriers and 2) $h_y \neq 0$ in the free F layer. The absence of either of these causes the supercurrent to revert to conventional behavior. In the short-junction regime where the Andreev bound states constitute the dominant contribution to the current (compared to the continuum current), barriers at both ferromagnetic interfaces are needed to produce the anomalous current: with either Z_1 or Z_2 set to zero, the $\sin\phi$ term in Equation (14.26) is absent. The fact that the anomalous supercurrent only appears when $h_y \neq 0$ indicates that the presence of an explicitly broken chiral spin symmetry is necessary. Interestingly, the direction of the current is actually controlled by the specific chirality, i.e., the sign of h_y. The ABS energies, the corresponding supercurrent, and the free energy for the trilayer Josephson junction are shown in Figure 14.5.

Having considered the equilibrium properties of the magnetically textured trilayer Josephson junction, we now look at the magnetization dynamics, for which the LLG equation (14.25) is solved numerically. The main ingredient which makes this possible is the effective field, which accounts for both the anisotropy terms and the ABS energies. This particular approach is valid when the magnetization dynamics are sufficiently slow compared to the rate at which the system relaxes to an equilibrium state [102]. For the simulations shown in Figure 14.5, we set $\beta_1 = \beta_2 = \pi/3$, $\Delta = 10^{-22}$ J, $\mu_0 = 10^{-6}$ H/m, $|M_0| = 10^5$ A/m, and the Gilbert damping parameter is set to $\alpha = 0.02$. In each case, the LLG equation is solved numerically and the stable state that arises when $t \to \infty$ and how it depends on the superconducting phase difference is identified. The initial condition for the magnetization of the free layer is taken to be along its easy anisotropy axis. Firstly, consider the case with anisotropy along the $\hat{y}$-direction shown in Figure 14.5. The stable state ($t \to \infty$) for each of the magnetization components and the effect of varying the anisotropy strength K is shown in (a), (b), and (c) of the bottom figure. The combined effect of exchange field and width of the ferromagnetic layer $\beta_3 \propto hL$ is shown in (d), (e), and (f), and the interface barrier transparency Z is shown in (g), (h), and (i). Several features can be noted. Whereas the qualitative behavior of the m_x (right panel, left column) and m_z (right panel, right column) components are equivalent, displaying a symmetry around $\phi = \pi$, the m_y (right panel, middle column) component behaves differently. For some parameter regimes, we observe very fast oscillations in the value of the stable state as a function of the superconducting phase difference. The reason for this can be traced back to a relation between the magnetization dynamics and the presence of an anomalous supercurrent in the system, and is discussed in detail in [83].

14.3.3 Spin-transfer torques tunable via the superconducting phase

The phenomenon of spin-transfer torques is generating much interest in spintronics since they involve the coupling between itinerant carriers (electrons or magnons) and collective magnetic order parameters and has found use in both magnetic random access memories and oscillator circuits [103, 104]. Spin-transfer torques result from the transfer of spin angular momentum from the (spin) current to the magnetic order parameter. While several works have considered spin transport and torques in heterostructures combining conventional *s*-wave superconductors with magnetic materials, much less is known about of how spin-transfer torques are manifested in materials which simultaneously display superconductivity and magnetism. This occurs in so-called ferromagnetic superconductors: uranium-based heavy-fermion compounds where superconductivity appears inside the magnetic part of the phase diagram. In these systems, it was shown in [105] that the spin-transfer torques depend on the phase of the superconducting pairing correlations. This can be utilized as an addi-

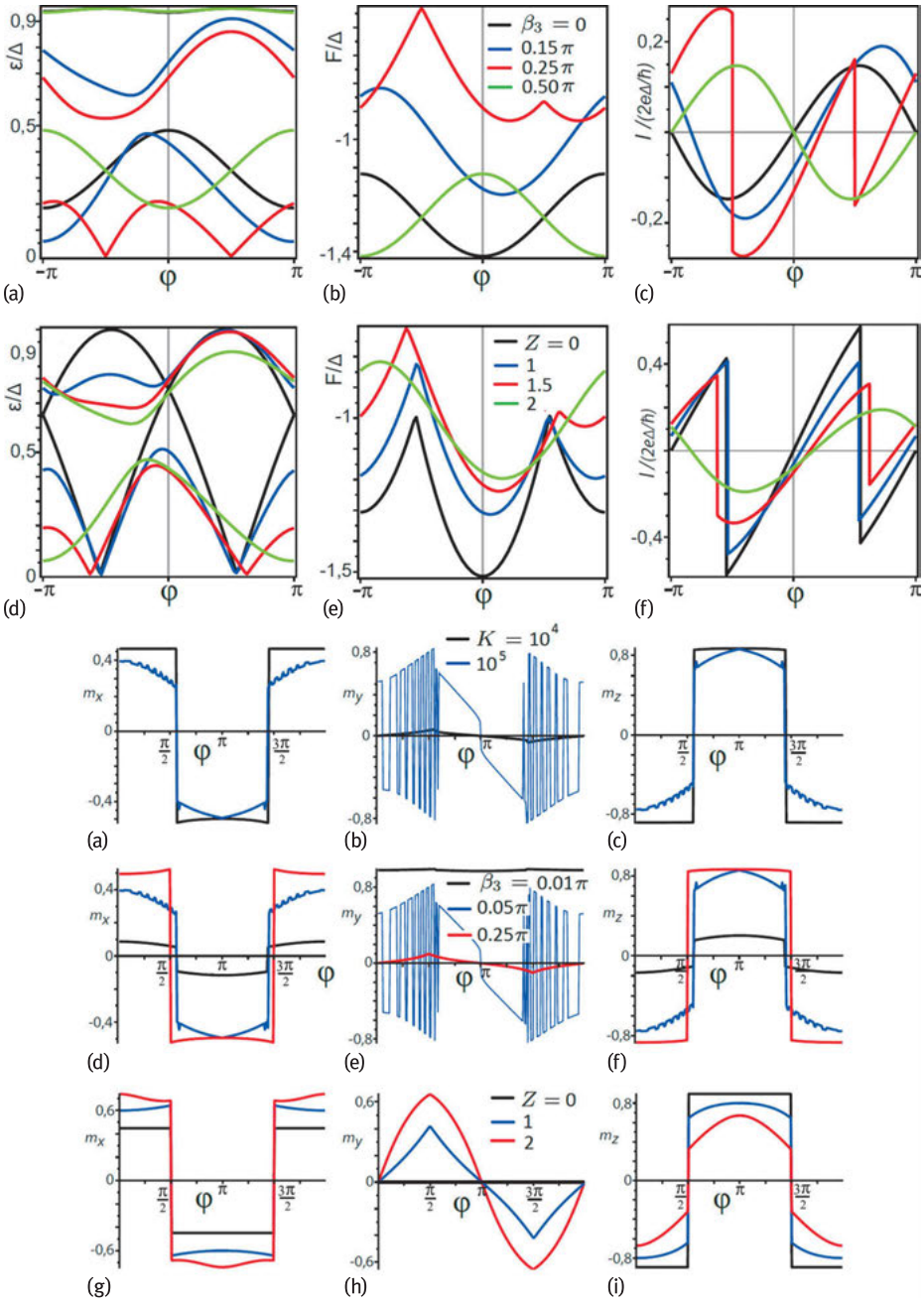

◂ **Fig. 14.5: Top figure.** (a,d): ABS energies and (b,e): free energy of the system versus superconducting phase difference. (c,f) Supercurrent-phase relation for the trilayered SFFFS structure. In all plots, $\beta_1 = \beta_2 = \pi/3$. In (a,b,c), $Z = 2$ and the effect of different values of β_3 is shown. For (d,e,f), $\beta_3 = 15\pi/100$ and the effect of a varying barrier potential Z is shown. **Bottom figure.** Stable magnetization state for $t \to \infty$ when $\mathbf{m}_3(t = 0) \parallel \hat{y}$. The components of the magnetization are given in the left (m_x), middle (m_y), and right (m_z) columns. For all panels, $\beta_1 = \beta_2 = \pi/3$. For (a,b,c): $\beta_3 = 5\pi/100$, $Z = 0.5$, and the effect of different values of the anisotropy constant K is illustrated. For (d,e,f): $Z = 0.5$, $K = 10^5$, and the effect of altering the β_3 parameter is shown. For (g,h,i): $\beta_3 = 25\pi/100$, $K = 10^5$, and the effect of different values of the barrier transparency Z is shown. K is given in units of J/m^3. Figure is adapted from [83].

tional way of controlling and detecting spin transport and magnetization dynamics and we now discuss the underlying principles for this effect.

To model the coexistence of bulk superconductivity and ferromagnetism, as experimentally verified in UGe_2 [106], URhGe [107], and UCoGe [108], we consider only equal spin-pairing triplet superconductivity: singlet pairing would not be able to survive the large Zeeman fields of order 70 meV in UGe_2 [106]. We first demonstrate that the out-of-equilibrium spin transfer in ferromagnetic superconductors is qualitatively different from what happens in conventional ferromagnets. Normally, the spin-transfer torque exerted on the magnetic order parameter is equal to the loss of transverse spin current inside the ferromagnet. This absorption takes place over a small distance from the interface region, typically of order a few Fermi wavelengths in strong ferromagnets where the exchange field makes up a considerable fraction of the Fermi level. In ferromagnetic superconductors, however, we find that the spin-transfer torque does not equal the loss of quasiparticle spin current. The reason for this may be understood by analyzing the spin continuity equation. We start by introducing the spin density $\boldsymbol{S}$ and the Hamiltonian H:

$$\boldsymbol{S} = \frac{1}{2}\psi^\dagger \begin{pmatrix} \sigma & 0 \\ 0 & -\sigma^* \end{pmatrix} \psi, \quad H = \begin{pmatrix} H_0 & \Delta \\ \Delta^* & -H_0^* \end{pmatrix}, \tag{14.27}$$

where $\hbar = 1$ and $H_0 = -\nabla^2/(2m) - \mu - \boldsymbol{h}\cdot\sigma$, $\Delta = \mathrm{diag}(\Delta_\uparrow, \Delta_\downarrow)$. Here, $\boldsymbol{h}$ is the exchange field, σ is a vector of Pauli matrices, and Δ_σ, $\sigma = \uparrow, \downarrow$ are the superconducting order parameters for majority and minority spin carriers. The Hamiltonian (14.27) determines the rate of change of the spin density:

$$\partial_t \boldsymbol{S} + \partial_i \boldsymbol{J}_S^i = \mathcal{S}_{\mathrm{super}} + \tau_{\mathrm{STT}}, \tag{14.28}$$

where we have defined

$$\begin{aligned} \boldsymbol{J}_S^i &= \frac{1}{2m}\mathrm{Im}\{\psi_1^\dagger \sigma \partial_i \psi_1 + \psi_2^\dagger \sigma^* \partial_i \psi_2\}, \\ \mathcal{S}_{\mathrm{super}} &= -\mathrm{Im}\{\psi_2^\dagger \Delta^* \sigma \psi_1 - \psi_1^\dagger \Delta \sigma^* \psi_2\}, \\ \tau_{\mathrm{STT}} &= \psi_1^\dagger [\sigma \times \mathbf{h}]\psi_1 - \psi_2^\dagger [\sigma^* \times \mathbf{h}]\psi_2 \end{aligned} \tag{14.29}$$

and ψ_1 and ψ_2 are electron- and hole-like 2×1 spinors constituting the total wavefunction, i.e., $\psi = (\psi_1, \psi_2)^{\mathrm{T}}$.

The rate of change of the spin-density terms entering the spin-continuity equation of Equation (14.28) are the quasiparticle spin-current tensor $\boldsymbol{J}_S$ (superscript i indicating its spatial components in Equation (14.28)), the spin supercurrent carried by the condensate $\mathcal{S}_{\mathrm{super}}$, and the spin-transfer torque exerted on the ferromagnetic order parameter τ_{STT}. The spin-transfer torque has a simple interpretation in the case of stationary transport in a normal metal-ferromagnet system: it is the loss of the transverse component of the spin current, $\partial_i \boldsymbol{J}_S^i = \tau_{\mathrm{STT}}$ since deep inside the ferromagnet only spins aligned with the local magnetization axis can exist. The total torque is $\int \tau_{\mathrm{STT}} = \boldsymbol{J}_S(\mathrm{F}) - \boldsymbol{J}_S(\mathrm{N})$ where $\boldsymbol{J}_S(\mathrm{N})$ is the spin current at the N-F interface and $\boldsymbol{J}_S(\mathrm{F})$ is the spin current in the bulk of the ferromagnet. In metallic ferromagnets which are in good electric contact with normal metals, the incoherence between the spin-up and spin-down states within the ferromagnet results in the transverse components of $\boldsymbol{J}_S(\mathrm{F})$ vanishing at length scales larger than the transverse decoherence length. Thus, $\int \tau_{\mathrm{STT}} = \boldsymbol{m} \times [\boldsymbol{m} \times \boldsymbol{J}_S(\mathrm{N})]$, which is well known [104].

In the present superconducting case, the situation becomes more complex. Since the components of the wavefunction ψ_1 and ψ_2 contain contributions from electron- and hole-like quasiparticles, Equation (14.28) shows that the torque is directly modified by superconducting correlations. In turn, these correlations are determined by the coherence factors and depend explicitly on the superconducting U(1) phases associated with each of the order parameters $\Delta_\sigma = |\Delta_\sigma| e^{i\phi_\sigma}$ in p-wave ferromagnetic superconductors. Consequently, the spin-transfer torque is sensitive to the superconducting phase. This should be viewed in contrast to e.g., the charge conductance which is insensitive to the U(1) phase. The origin of this effect is that the torque acquires a contribution from interference terms of the propagation of electron- and hole-like excitations. Since these excitations have different U(1) superconducting phases due to the spin-resolved condensate, the torque will depend explicitly on the internal phase difference between the two spin condensates. This was analytically verified by direct computation in [105]. It is important to note that since part of the spin current is carried by the condensate via $\mathcal{S}_{\mathrm{super}}$, the loss of the quasiparticle spin current is not fully compensated by the torque τ_{STT} exerted on the ferromagnetic order parameter.

It follows from the above discussion that the spin-transfer torque is qualitatively different in ferromagnetic superconductors as compared to ferromagnets, because of the presence of particle-hole interference of the quasiparticle waves which is unique in the superconducting state: it vanishes when $\Delta_\sigma \to 0$. More specifically, the injected spin current causes transmission of both electron-like and hole-like quasiparticles into the superconductor with weight denoted u and v, respectively. The interference between two electron-like waves (or two hole-like waves) gives rise to the usual spin-transfer torque oscillating on the length scale λ_h. In addition, however, there are extra terms compared to the nonsuperconducting case proportional to $u^* v$ which represent particle-hole interference. This also gives rise to a different length scale than the

one relevant for conventional spin-transfer torque since hole-like waves have opposite momentum relative to their group velocity. Consequently, they interfere with the electron-like waves in a way that cancels out the exchange-field dependence on the oscillation length. A unique aspect of the spin-transfer torque acting on a ferromagnetic superconductor is that the torque itself might be able to rotate the superconducting order parameter [109] due to the coupling between it and the local magnetization. The latter, having a spin-triplet symmetry, is characterized by the so-called $\boldsymbol{d_k}$-vector formalism [26]. For a sufficiently large torque acting on the magnetic order parameter, one could expect the superconducting order parameter to start rotating in spin space as well due to the coupling $\langle \boldsymbol{S} \rangle \cdot \boldsymbol{M}$ between the spins of the Cooper pairs $\langle \boldsymbol{S} \rangle \propto \mathrm{i}\boldsymbol{d_k} \times \boldsymbol{d_k^*}$ and the magnetization $\boldsymbol{M}$.

The fact that the spin-transfer torque depends on the difference $\phi = \phi_\uparrow - \phi_\downarrow$ between the spontaneously broken U(1) phases of the superconducting order parameters Δ_σ may be understood as follows. For longitudinally polarized spin currents, the spin supercurrent is carried by the condensate with phase $\phi_\uparrow$ and the condensate with phase $\phi_\downarrow$ separately (no superposition occurs). This changes when a transverse spin current is injected as in the present case, with a spin polarization at an angle θ with respect to the magnetic order parameter. This corresponds to a noncollinear superposition of quasiparticles from the two spin branches of the condensate. Consequently, the phase difference appears in the expression for the spin-transfer torque, offering a possible experimental probe for the relative phase difference ϕ.

Acknowledgment: We would like to thank in particular K. Halterman, J. A. Ouassou, I. Gomperud, I. Kulagina, J. Robinson, A. Di Bernardo, M. Blamire, A. Pal, N. Banerjee, M. Eschrig, and V. Risinggård for fruitful collaboration and helpful discussions on the topics presented herein.

Bibliography

[1] Linder J, Robinson JWA. Superconducting spintronics. Nat. Phys. 11:307, 2015.
[2] Bergeret FS, Volkov AF, Efetov KB. Long-Range Proximity Effects in Superconductor-Ferromagnet Structures. Phys. Rev. Lett. 86:4096, 2001.
[3] Buzdin AI. Proximity effects in superconductor-ferromagnet heterostructures. Rev. Mod. Phys. 77:935, 2005.
[4] Bergeret FS, Volkov AF, Efetov KB. Odd triplet superconductivity and related phenomena in superconductor-ferromagnet structures. Rev. Mod. Phys. 77:1321, 2005.
[5] Eschrig M. Spin-polarized supercurrents for spintronics: a review of current progress. Rep. Prog. Phys. 78:10, 2015.
[6] Blamire MG, Robinson JWA. The interface between superconductivity and magnetism: understanding and device prospects. J. Phys. Cond. Mat. 26:45, 2014.
[7] Grein R, Eschrig M, Metalidis G, Schön G. Spin-Dependent Cooper Pair Phase and Pure Spin Supercurrents in Strongly Polarized Ferromagnets. Phys. Rev. Lett. 102:227005, 2009.

[8] Alidoust M, Linder J, Rashedi G, Yokoyama T, Sudbø A. Spin-polarized Josephson current in superconductor/ferromagnet/superconductor junctions with inhomogeneous magnetization. Phys. Rev. B 81:014512, 2010.
[9] Shomali Z, Zareyan M, Belzig W. Spin supercurrent in Josephson contacts with noncollinear ferromagnets. New J. Phys. 13:083033, 2011.
[10] Moor A, Volkov A, Efetov KB. Nematic versus ferromagnetic spin filtering of triplet Cooper pairs in superconducting spintronics. Phys. Rev. B 92:180506(R), 2015.
[11] Halterman K, Valls OT, Wu C-T. Charge and spin currents in ferromagnetic Josephson junctions. Phys. Rev. B 92:174516, 2015.
[12] Keizer RS, Goennenwein STB, Klapwijk TM, Miao G, Xiao G, Gupta A. A spin triplet supercurrent through the half-metallic ferromagnet CrO2. Nature 439:825–827, 2006.
[13] Khaire ST, Khasawneh M, Pratt WP Jr, Birge NO. Observation of spin-triplet superconductivity in Co-based Josephson junctions. Phys. Rev. Lett. 104:137002, 2010.
[14] Robinson JWA, Witt JDS, Blamire MG. Controlled injection of spin-triplet supercurrents into a strong ferromagnet. Science 329:59–61, 2010.
[15] Di Bernardo A, Diesch S, Gu, Y., Linder J, Divitini G, Ducato C, Scheer E, Blamire MG, Robinson JWA. Signature of Magnetic-Dependent Gapless Odd frequency States at Superconductor/Ferromagnet Interfaces. Nat. Commun. 6:8053, 2015.
[16] Kalcheim Y, Millo O, Di Bernardo A, Pal A, Robinson JWA. Inverse proximity effect at superconductor-ferromagnet interfaces: Evidence for induced triplet pairing in the superconductor. Phys. Rev. B 92:060501(R), 2015.
[17] Di Bernardo A, Salman Z, Wang XL, Amado M, Egilmez M, Flokstra MG, Suter A, Lee SL, Zhao JH, Proksch T, Morenzoni E, Blamire MG, Linder J, Robinson JWA. Intrinsic Paramagnetic Meissner Effect Due to *s*-Wave Odd-Frequency Superconductivity. Phys. Rev. X 5:041021, 2015.
[18] Bergeret FS, Tokatly IV. Singlet-triplet conversion and the long-range proximity effect in superconductor-ferromagnet structures with generic spin dependent fields. Phys. Rev. Lett. 110:117003, 2013.
[19] Bergeret FS, Tokatly IV. Spin-orbit coupling as a source of long-range triplet proximity effect in superconductor-ferromagnet hybrid structures. Phys. Rev. B 89:134517, 2014.
[20] Rammer J, Smith H. Quantum field-theoretical methods in transport theory of metals. Rev. Mod. Phys. 58:323, 1986.
[21] Belzig W, Wilhelm FK, Bruder C, Schön G, & Zaikin AD. Quasiclassical Green's function approach to mesoscopic superconductivity. Superlattice. Microst. 25:1251, 1999.
[22] Eschrig M, Kopu J, Cuevas JC, Schön G. Theory of Half-Metal/Superconductor Heterostructures. Phys. Rev. Lett. 90:137003, 2003.
[23] Annunziata G, Manske D, Linder J. Proximity effect with noncentrosymmetric superconductors. Phys. Rev. B 86:174514, 2012.
[24] Rashba E. Fiz. Tverd. Tela (Leningrad) 2:1224, 1960 [Properties of semiconductors with an extremum loop. 1. Cyclotron and combinational resonance in a magnetic field perpendicular to the plane of the loop. Sov. Phys. Solid State 2:1109, 1960].
[25] Gor'kov LP, Rashba EI. Superconducting 2D System with Lifted Spin Degeneracy: Mixed Singlet-Triplet State. Phys. Rev. Lett. 87:037004, 2001.
[26] Leggett AK. A theoretical description of the new phases of liquid He3. Rev. Mod. Phys. 47:331, 1975.
[27] D'yakonov MI, Perel VI, Spin Orientation of Electrons Associated with the Interband Absorption of Light in Semiconductors. Sov. Phys. JETP 33:1053, 1971; D'yakonov MI, Perel VI. Current-induced spin orientation of electrons in semiconductors. Phys. Lett. A 35:459, 1971.

[28] Usadel K. Generalized Diffusion Equation for Superconducting Alloys. Phys. Rev. Lett. 25:507, 1970.
[29] Gu JY, You C-Y, Jiang JS, Pearson J, Bazaliy YaB, Bader SD. Magnetization-Orientation Dependence of the Superconducting Transition Temperature in the Ferromagnet-Superconductor-Ferromagnet System: CuNi/Nb/CuNi. Phys. Rev. Lett. 89:267001, 2002.
[30] Moraru I, Pratt WP Jr, Birge N. Magnetization-Dependent Tc Shift in Ferromagnet/Superconductor/Ferromagnet Trilayers with a Strong Ferromagnet. Phys. Rev. Lett. 96:037004, 2006.
[31] Zhu J, Krivorotov IN, Halterman K, Valls OT. Angular Dependence of the Superconducting Transition Temperature in Ferromagnet-Superconductor-Ferromagnet Trilayers. Phys. Rev. Lett. 105:207002, 2010.
[32] Leksin PV, Garif'yanov NN, Garifullin IA, Fominov YaV, Schumann J, Krupskaya Y, Kataev V, Schmidt OG, Büchner B. Evidence for Triplet Superconductivity in a Superconductor-Ferromagnet Spin Valve. Phys. Rev. Lett. 109:057005, 2012.
[33] Banerjee N, Smiet CB, Smits RGJ, Ozaeta A, Bergeret FS, Blamire MG, Robinson JWA. Evidence for spin selectivity of triplet pairs in superconducting spin valves. Nature Commun. 5:3048, 2014.
[34] Jacobsen SH, Ouassou JA, Linder J. Critical temperature and tunneling spectroscopy of superconductor-ferromagnet hybrids with intrinsic Rashba–Dresselhaus spin-orbit coupling. Phys. Rev. B 92:024510, 2015.
[35] Dresselhaus G. Spin-Orbit Coupling Effects in Zinc Blende Structures. Phys. Rev. 100:580, 1955.
[36] Bauer E, Sigrist M. Non-Centrosymmetric Superconductors: Introduction and overview. Springer, 2012.
[37] Samokhin KV. Spin–orbit coupling and semiclassical electron dynamics in noncentrosymmetric metals. Ann. Phys. 324:2385, 2009.
[38] Hammer JC, Cuevas JC, Bergeret FS, Belzig W. Density of states and supercurrent in diffusive SNS junctions: Roles of nonideal interfaces and spin-flip scattering. Phys. Rev. B 76:064514, 2007.
[39] Le Sueur H, Joyez P, Pothier H, Urbina C, Esteve D. Phase Controlled Superconducting Proximity Effect Probed by Tunneling Spectroscopy. Phys. Rev. Lett. 100:197002, 2008.
[40] Zhou F, Charlat P, Pannetier B. Density of States in Superconductor-Normal Metal-Superconductor Junctions. J. Low Temp. Phys. 110:841, 1998.
[41] Jacobsen SH, Linder J. Giant triplet proximity effect in π-biased Josephson Junctions with spin-orbit coupling. Phys. Rev. B 92:024501, 2015.
[42] Kupriyanov MY, Lukichev VF. Influence of boundary transparency on the critical current of "dirty" SS'S structures. Sov. Phys. JETP 67:1163, 1988.
[43] Bardeen J, Cooper LN, Schrieffer JR. Theory of Superconductivity. Phys. Rev. 108:1175, 1957.
[44] Kontos T, Aprili M, Lesueur J, Grison X, Inhomogeneous Superconductivity Induced in a Ferromagnet by Proximity Effect. Phys. Rev. Lett. 86:304, 2001; Ryazanov VV, Oboznov VA, Rusanov AYu, Veretennikov AV, Golubov AA, Aarts J. Coupling of Two Superconductors through a Ferromagnet: Evidence for a π Junction. Phys. Rev. Lett. 86:2427, 2001.
[45] SanGiorgio P, Reymond S, Beasley MR, Kwon JH, Char K. Anomalous Double Peak Structure in Superconductor/Ferromagnet Tunneling Density of States. Phys. Rev. Lett. 100:237002, 2008.
[46] Tedrow PM, Meservey R. Spin-dependent tunneling into ferromagnetic nickel. Phys. Rev. Lett. 26:192–195, 1971.
[47] Tedrow PM, Meservey R. Spin polarization of electrons tunneling from films of Fe, Co, Ni, and Gd. Phys. Rev. B 7:318–326, 1973.
[48] Tedrow PM, Meservey R. Spin-polarized electron tunneling. Phys. Rep. 238:173–243, 1994.

[49] Johnson M, Silsbee RH. Interfacial charge-spin coupling: Injection and detection of spin magnetization in metals. Phys. Rev. Lett. 55:1790–1793, 1985.
[50] Li B, Roschewsky N, Assaf BA, Eich M, Epstein-Martin M, Heiman D, Münzenberg M, Moodera JS. Superconducting spin switch with infinite magnetoresistance induced by an internal exchange field. Phys. Rev. Lett. 110:097001, 2013.
[51] Yang H, Yang S-H, Takahashi S, Maekawa S, Parkin SSP. Extremely long quasiparticle spin lifetimes in superconducting aluminium using MgO tunnel spin injectors. Nature Mater. 9:586–593, 2010.
[52] Quay CHL, Chevallier D, Bena C, Aprili M. Spin imbalance and spin-charge separation in a mesoscopic superconductor. Nature Phys. 9:84–88, 2013.
[53] Wakamura T, Omori Y, Niimi Y, Takahashi S, Fujimaki A, Maekawa S, Otani Y. Quasiparticle-mediated spin Hall effect in a superconductor. Nature Materials 14:675–678, 2015.
[54] Kolenda S, Wolf MJ, Beckmann D. Observation of thermoelectric currents in high-field superconductor-ferromagnet tunnel junctions. Phys. Rev. Lett. 116:097001, 2016.
[55] Sprungmann D, Westerholt K, Zabel H, Weides M, Kohlstedt H. Evidence for triplet superconductivity in Josephson junctions with barriers of the ferromagnetic Heusler alloy Cu2MnAl. Phys. Rev. B 82:060505(R), 2010.
[56] Houzet M, Buzdin AI. Long range triplet Josephson effect through a ferromagnetic trilayer. Phys. Rev. B 76:060504(R), 2007.
[57] Trifunovic L. Long-Range Superharmonic Josephson Current. Phys. Rev. Lett. 107:047001, 2011.
[58] Fogelstrom M. Josephson currents through spin-active interfaces. Phys. Rev. B 62:11812, 2000.
[59] Bobkova IV, Bobkov AM. Long-Range Proximity Effect for Opposite-Spin Pairs in Superconductor-Ferromagnet Heterostructures Under Nonequilibrium Quasiparticle Distribution. Phys. Rev. Lett. 108:197002, 2012.
[60] Gomperud I, Linder J. Spin supercurrent and phase-tunable triplet Cooper pairs via magnetic insulators. Phys. Rev. B 92:035416, 2015.
[61] Chandrasekhar V. An introduction to the quasiclassical theory of superconductivity for diffusive proximity-coupled systems. In: Bennemann K, Ketterson J (eds). The Physics of Superconductors, Vol II., Springer, 2004.
[62] Schopohl N, Maki K. Quasiparticle spectrum around a vortex line in a d-wave superconductor. Phys. Rev. B. 52:490, 1995; Schopohl, N. arXiv:cond-mat/9804064.
[63] Cottet A, Huertas-Hernando D, Belzig W, Nazarov YV. Spin-dependent boundary conditions for isotropic superconducting Green's functions. Phys. Rev. B 80:184511, 2009.
[64] Eschrig M, Cottet A, Belzig W, Linder J. General boundary conditions for quasiclassical theory of superconductivity in the diffusive limit: application to strongly spin-polarized systems. New J. Phys. 17:083037, 2015.
[65] Yamashita T, Takahashi S, Imamura H, Maekawa S. Spin transport and relaxation in superconductors. Phys. Rev. B 65:172509, 2002.
[66] Takahashi S, Imamura H, Maekawa S. Spin Imbalance and Magnetoresistance in Ferromagnet/Superconductor/Ferromagnet Double Tunnel Junctions. Phys. Rev. Lett. 82:3911, 1999.
[67] Clogston M. Upper Limit for the Critical Field in Hard Superconductors. Phys. Rev. Lett. 9:266, 1962.
[68] Chandrasekhar BS. A note on the maximum critical field of high-field superconductors. Appl. Phys. Lett. 1:7, 1962.
[69] Hübler F, Wolf MJ, Beckmann D, v. Löhneysen H. Long-range spin-polarized quasiparticle transport in mesoscopic Al superconductors with a Zeeman splitting. Phys. Rev. Lett. 109:207001, 2012.

[70] Poli N, Morten JP, Urech M, Brataas A, Haviland DB, Korenivski V. Spin injection and relaxation in a mesoscopic superconductor. Phys. Rev. Lett. 100:136601, 2008.
[71] Morten JP, Brataas A, Belzig W. Spin transport in diffusive superconductors. Phys. Rev. B 70:212508, 2004.
[72] Wakamura T, Hasegawa N, Ohnishi K, Niimi Y, Otani Y. Spin Injection into a Superconductor with Strong Spin-Orbit Coupling. Phys. Rev. Lett. 112:036602, 2014.
[73] Baek B, Rippard WH, Pufall MR, Benz SP, Russek SE, Rogalla H, Dresselhaus PD. Spin-Transfer Torque Switching in Nanopillar Superconducting-Magnetic Hybrid Josephson Junctions. Phys. Rev. Applied 3:011001, 2015.
[74] Linder J, Halterman K. Superconducting spintronics with magnetic domain walls. Phys. Rev. B 90:104502, 2014.
[75] Robinson JWA, Chiodi F, Halasz GB, Egilmez M, Blamire MG. Supercurrent enhancement in Bloch domain walls. Scientific Reports 2:699, 2012.
[76] Schryer NL, Walker LR. The motion of 180° domain walls in uniform dc magnetic fields. J. Appl. Phys. 45:5406, 1974.
[77] Kontos T, Aprili M, Lesueur J, Grison X, Dumoulin L. Superconducting Proximity Effect at the Paramagnetic-Ferromagnetic Transition. Phys. Rev. Lett. 93:137001, 2004.
[78] Blanter YaM, Hekking FWJ. Supercurrent in long SFFS junctions with antiparallel domain configuration. Phys. Rev. B 69:024525, 2004.
[79] Waintal X, Brouwer PW. Magnetic exchange interaction induced by a Josephson current. Phys. Rev. B 65:054407, 2002.
[80] Zhao E, Sauls JA. Theory of Nonequilibrium Spin Transport and Spin Transfer Torque in Superconducting-Ferromagnetic Nanostructures. Phys. Rev. B 78:174511, 2008.
[81] Linder J, Yokoyama T. Supercurrent-induced magnetization dynamics. Phys. Rev. B 83:012501, 2011.
[82] Sacramento PD, Fernandes Silva LC, Nunes GS, Araujo MAN, Vieira VR, Supercurrent-induced domain wall motion. Phys. Rev. B 83:054403, 2011; Sacramento PD, Araujo MAN. Spin torque on magnetic domain walls exerted by supercurrents, Eur. Phys. J. B 76:251, 2010.
[83] Kulagina I, Linder J. Spin Supercurrent, Magnetization Dynamics, and ϕ-State in Spin-Textured Josephson Junctions. Phys. Rev. B 90:054504, 2014.
[84] Oboznov VA, Bol'ginov VV, Feofanov AK, Ryazanov VV, Buzdin AI. Thickness Dependence of the Josephson Ground States of Superconductor-Ferromagnet-Superconductor Junctions. Phys. Rev. Lett. 96:197003, 2006.
[85] Himeno A, Ono T, Nasu S, Shigeto K, Mibu K, Shinjo T. Dynamics of a magnetic domain wall in magnetic wires with an artificial neck. J. Appl. Phys. 93:8430, 2003.
[86] Boulle O, Malinowski G, Kläui M. Current-induced domain wall motion in nanoscale ferromagnetic elements. Mater. Sci. Eng., R 72:159, 2011.
[87] Ebels U, Radulescu A, Henry Y, Piraux L, Ounadjela K. Spin Accumulation and Domain Wall Magnetoresistance in 35 nm Co Wires. Phys. Rev. Lett. 84:983, 2000.
[88] Konschelle F, Buzdin A. Magnetic Moment Manipulation by a Josephson Current. Phys. Rev. Lett. 102:017001, 2009.
[89] Teber S, Holmqvist C. Fogelstrom. Transport and magnetization dynamics in a superconductor/single-molecule magnet/superconductor junction. Phys. Rev. B 81:174503, 2010.
[90] Holmqvist C, Teber S. and Fogelstrom. Nonequilibrium effects in a Josephson junction coupled to a precessing spin. Phys. Rev. B 83:104521, 2011.
[91] Houzet M. Ferromagnetic Josephson Junction with Precessing Magnetization. Phys. Rev. Lett. 101:057009, 2008.
[92] Yokoyama T, Tserkovnyak Y. Tuning odd triplet superconductivity by spin pumping. Phys. Rev. B 80:104416, 2009.

[93] Buzdin A. Direct Coupling Between Magnetism and Superconducting Current in the Josephson φ_0 Junction. Phys. Rev. Lett. 101:107005, 2008.
[94] Blonder GE, Tinkham M, Klapwijk TM. Transition from metallic to tunneling regimes in superconducting microconstrictions: Excess current, charge imbalance, and supercurrent conversion. Phys. Rev. B 25:4515, 1982.
[95] Asano Y, Sawa Y, Tanaka Y, Golubov AA. Odd-frequency pairs and Josephson current through a strong ferromagnet. Phys. Rev. B 76:224525, 2007.
[96] Margaris I, Paltoglou V, Flytzanis N. Zero phase difference supercurrent in ferromagnetic Josephson junctions. J. Phys.: Condens. Matter 22:445701, 2010.
[97] Szombati DB, Nadj-Perge S, Car D, Plissard SR, Bakkers EPAM, Kouwenhoven LP. Josephson φ_0-junction in nanowire quantum dots. Nature Physics 12:568, 2016.
[98] deGennes PG. Superconductivity Of Metals And Alloys. Westview Press, 1999.
[99] Beenakker CWJ, Universal limit of critical-current fluctuations in mesoscopic Josephson junctions. Phys. Rev. Lett. 67:3836, 1991; Beenakker CWJ, van Houten H. Josephson current through a superconducting quantum point contact shorter than the coherence length. ibid. 66:3056, 1991.
[100] Jacobsen SH, Kulagina I, Linder J. Controlling superconducting spin flow with spin-flip immunity using a single homogeneous ferromagnet. Sci. Rep. 6:23926, 2016.
[101] Landau LD, Lifshitz E, On the theory of the dispersion of magnetic permeability in ferromagnetic bodies. Phys. Z. Sowjetunion 8:153, 1935; Gilbert TL. A phenomenological theory of damping in ferromagnetic materials. IEEE Trans. Magn. 40:3443, 2004.
[102] Tserkovnyak Y, Brataas A, Bauer GEW, Halperin BI. Nonlocal magnetization dynamics in ferromagnetic heterostructures. Rev. Mod. Phys. 77:1375, 2005.
[103] Slonczewski JC, Current-driven excitation of magnetic multilayers. J. Magn. Magn. Mater. 159:L1, 1996; Berger L. Emission of spin waves by a magnetic multilayer traversed by a current. Phys. Rev. B 54:9353, 1996.
[104] Ralph DC, Stiles MD, Spin transfer torques. J. Magn. Magn. Mat. 320:1190, 2008; Brataas A, Kent AD, Ohno H. Current-induced torques in magnetic materials. Nature Mater. 11:372, 2012.
[105] Linder J, Brataas A, Shomali Z, Zareyan M. Spin-Transfer and Exchange Torques in Ferromagnetic Superconductors. Phys. Rev. Lett. 109:237206, 2012.
[106] Saxena SS, Agarwal P, Ahilan K, Grosche FM, Haselwimmer RKW, Steiner MJ, Pugh E, Walker IR, Julian SR, Monthoux P, Lonzarich GG, Huxley A, Sheikin I, Braithwaite D, Flouquet J. Superconductivity on the border of itinerant-electron ferromagnetism in UGe_2. Nature (London) 406:587, 2000.
[107] Aoki D, Huxley A, Ressouche E, Braithwaite D, Flouquet J, Brison JP, Lhotel E, Paulsen C. Coexistence of superconductivity and ferromagnetism in URhGe. Nature (London) 413:613, 2001.
[108] Huy NT, Gasparini A, de Nijs DE, Huang Y, Klaasse JCP, Gortenmulder T, de Visser A, Hamann A, Görlach T, v. Löhneysen H. Superconductivity on the Border of Weak Itinerant Ferromagnetism in UCoGe. Phys. Rev. Lett. 99:067006, 2007.
[109] Brataas A, Tserkovnyak Y. Spin and Charge Pumping by Ferromagnetic-Superconductor Order Parameters. Phys. Rev. Lett. 93:087201, 2004.